OXFORD

Journal of Petrology, 2022, **63**, 1–22
https://doi.org/10.1093/petrology/egac110
Original Manuscript

Kelyphite Textures Experimentally Reproduced through Garnet Breakdown in the Presence of a Melt Phase

Isra S Ezad[1,2,*], David P Dobson[2], Andrew R Thomson[2], Eleanor S Jennings[3] and Simon A Hunt[2,4] and John P Brodholt[2]

[1] School of Natural Sciences, 12 Wallys Walk, Macquarie University, North Ryde, 2019, Sydney, NSW, Australia
[2]Department of Earth Sciences, University College London, Gower Street, London, WC1E 6BT, United Kingdom
[3]Department of Earth and Planetary Sciences, Birkbeck College, University of London, Malet Street, Bloomsbury, London, WC1E 7HX, United Kingdom
[4]Department of Materials, The University of Manchester, Oxford Road, Manchester, M13 9PL, United Kingdom

*Corresponding author: School of Natural Sciences, 12 Wallys Walk, Macquarie University, North Ryde, 2019, Sydney, NSW, Australia. E-mail: isra.ezad@mq.edu.au

Abstract

Complex multiphase reaction rims that form during garnet breakdown are known as kelyphite coronae and are common amongst exhumed mantle xenoliths. It has long been established that a reaction of garnet and olivine produces kelyphite corona consisting of spinel and pyroxenes, and that preservation of high-pressure garnet cores requires sufficiently rapid uplift of material through the spinel lherzolite stability field from depths of at least 60 km. We present new high-pressure, high-temperature experiments of garnet breakdown in the spinel–lherzolite stability field demonstrating that a series of cascading reactions can reproduce the multilayer, multiphase kelyphites seen in nature. In all experiments where breakdown occurred, a melt appears to have moderated the reactions towards equilibrium; we believe this to be the first experimental confirmation of the importance of such melts in garnet breakdown reactions. In our experiments at least three distinct zones of concentric kelyphite growth can occur at a single pressure, temperature condition; we suggest, therefore, that such kelyphites seen in natural samples do not have to be caused by a multistage uplift path as is often assumed. Kelyphitic coronae surrounding garnet have previously been used to estimate uplift rates; however, the lack of kinetic data for relevant exhumation reactions has limited their use for *PTt* pathway estimations and the understanding of emplacement mechanisms. In order to constrain accurate *PTt* pathways we use reaction rim thickness as a proxy for reaction progress and present preliminary results for the kinetics of garnet breakdown.

Keywords: kimberlite, peridotite, pyroxene, xenolith, P–T conditions, spinel, experimental petrology, garnet

INTRODUCTION

Garnet bearing mantle xenoliths are relatively rare and as a consequence their mineralogy, phase relations, and geothermobarometry have been subject to extensive research (e.g. Kushiro & Yoder, 1966; Carswell & Dawson, 1970; Macgregor, 1970; Lock & Dawson, 1980; Irifune, 1987; Clarke & Powell, 1991; Chakraborty & Ganguly, 1992; Ai, 1994; Karato *et al.*, 1995; Atzori *et al.*, 1999; Godard & Martin, 2000; Keankeo *et al.*, 2000; Medaris *et al.*, 2005; Dégi *et al.*, 2010; Su *et al.*, 2011). Their rarity is readily demonstrated by an assessment of their geological provenance: nearly all garnet lherzolite xenoliths are recovered from kimberlitic eruptions of Archean and Proterozoic age, whereas spinel lherzolite assemblages occur throughout geological time in orogenic massifs and alkali basalt volcanic eruptions (Lock & Dawson, 1980; Bjerg *et al.*, 2009; Su *et al.*, 2011). Infrequent occurrences of garnet lherzolite have been documented in alkali basalts from the Mesozoic and Cenozoic (Medaris *et al.*, 2005; Obata *et al.*, 2013; Špaček *et al.*, 2013). Garnet bearing mantle xenoliths are exhumed to the surface by violent processes at high temperatures (1000–1200°C) from minimum depths coinciding with the garnet to spinel lherzolite transition (50 to 80 km) (Peslier *et al.*, 2008; Kavanagh & Sparks, 2009; Špaček *et al.*, 2013). These high temperatures likely enhance the retrogression of garnet, so 'rapid' exhumation is inferred to be essential for successful recovery of unreacted garnet to Earth's surface.

Indeed, nearly all examples of garnet lherzolite exhibit textural evidence of partial or complete retrogression of garnet (Carswell & Dawson, 1970; Reid & Dawson, 1972; Basu & MacGregor, 1975; Lock & Dawson, 1980; Clarke & Powell, 1991; Atzori *et al.*, 1999; Grégoire *et al.*, 2005; Dégi *et al.*, 2010). These coronae are commonly referred to as kelyphite and are indicative of retrograde reactions taking place within the garnet during exhumation (Carswell & Dawson, 1970; Reid & Dawson, 1972).

The breakdown reactions can be generalised into two forms, the first involving excess olivine:

$$Garnet + Olivine \rightleftarrows Spinel + Orthopyroxene \pm Clinopyroxene \quad (1)$$

and the second, in the absence of olivine:

$$Garnet \rightleftarrows Spinel + Orthopyroxene + Anorthite \pm Clinopyroxene \quad (2)$$

where the growth of clinopyroxene and anorthite is dependent on the grossular content of the parent garnet. Kelyphite produced by Reaction 2 can be further subdivided into those that form in an isochemical (chemically closed) or non-isochemical (chemically open) type (Obata *et al.*, 2014, 2013; Obata, 2016). The intricacies of these subdivisions are discussed in detail by Obata *et al.* (2013). Some of the most common textures following Reactions 1 and 2 are discussed by Obata (2011) and Obata & Ozawa (2011).

Reid & Dawson (1972) were the first to ascribe the development of kelyphitic coronae in peridotite xenoliths to be the result of

Received: August 7, 2019. **Revised:** October 4, 2022

retrogressed garnet in the presence of olivine. They found three primary minerals in the interior of fresh unaltered kelyphite; spinel, orthopyroxene and clinopyroxene, which were surrounded by olivine. Reid & Dawson (1972) observed many coronae were subdivided into concentric zones surrounding relic garnet, each with a distinctive grain size and modal phase proportion. Subsequent work has shown that concentric zones surrounding relic garnet are common, with the number and type of zones depending on alteration, presence of melt, bulk composition, exhumation history, phases present and textural characteristics of those phases (Hunter & Taylor, 1982; Brearley & Scarfe, 1986; Godard & Martin, 2000; Špaček *et al.*, 2013).

Kelyphite coronae are observed most frequently in mantle xenoliths derived from unusual volcanic settings examples of which include carbonatitic fields, for example, Lashaine and Tanzania (Reid & Dawson, 1972); kimberlite eruptions, for example, Lesotho (Lock & Dawson, 1980; Richardson *et al.*, 1985); and nephelinitic breccia pipes, for example, New South Wales (Keankeo *et al.*, 2000). Aside from these special geologic settings there have been occasional documented occurrences of reaction coronae surrounding garnet in orogenic belts and alkali basalts (Medaris *et al.*, 2005; Špaček *et al.*, 2013). The relationship of post-garnet retrograde reaction textures to exhumation processes has been widely discussed (Medaris *et al.*, 2005; Obata & Ozawa, 2011; Obata *et al.*, 2013; Špaček *et al.*, 2013), and their application as indicators of pressure–temperature–time (*PTt*) pathways remains challenging. Amongst the interpretations of post-garnet textures, a significant decompression upon uplift is favoured in inducing garnet breakdown, leading to the array of textures seen in natural garnet peridotite (Reid & Dawson, 1972; Lock & Dawson, 1980; Godard & Martin, 2000).

The previous experimental study of Obata *et al.* (2014) investigated the generation of textures associated with garnet breakdown, successfully reproducing kelyphite textures associated with Reaction 2. However, this study did not constrain the associated reaction kinetics. Kinetics of the spinel to garnet reaction (backward reaction of Reaction 1) were studied by Nagayoshi *et al.* (2016), but these failed to consistently produce olivine as a reaction product; only one experiment with the full three-phase assemblage expected during the spinel to garnet reaction in peridotites was reported such that kinetic constraints remain highly limited. Our study extends the experimental data, including kinetic information, for retrograde garnet textures formed during equilibration in the spinel lherzolite field. In addition to reproducing kelyphitic textures observed in nature, this study introduces a new series of reaction pathways for garnet breakdown including the presence of a melt phase that mediates garnet retrogression through incongruent melting (Hunter & Taylor, 1982).

The presence of transient/metastable melts partaking in other breakdown reactions is well documented. Rubie & Brearley (1987) reported metastable melting during breakdown of quartz and muscovite, while Johannes (1980) described metastable melting of granitic compositions as a rock forming process in nature.

Our study is not the first proposal of such a melt or liquid phase contributing to garnet breakdown and kelyphite formation (Hunter & Taylor, 1982; Brearley & Scarfe, 1986), but we believe these experiments are the first reproduction of kelyphite textures co-existing with *in situ* melts, akin to those observed in nature (Hunter & Taylor, 1982; Brearley & Scarfe, 1986; Špaček *et al.*, 2013). This study discusses the possible importance of this melt during garnet breakdown, which until now has been almost impossible to identify as there are no chemical fingerprints of the involvement of a melt phase as noted by Špaček *et al.* (2013).

Throughout this paper we describe kelyphite textures produced during high-pressure, high-temperature experiments, demonstrating that garnet breakdown is not a simple, single stage, olivine + garnet reaction and provide evidence for the necessity of melt during garnet breakdown in nature.

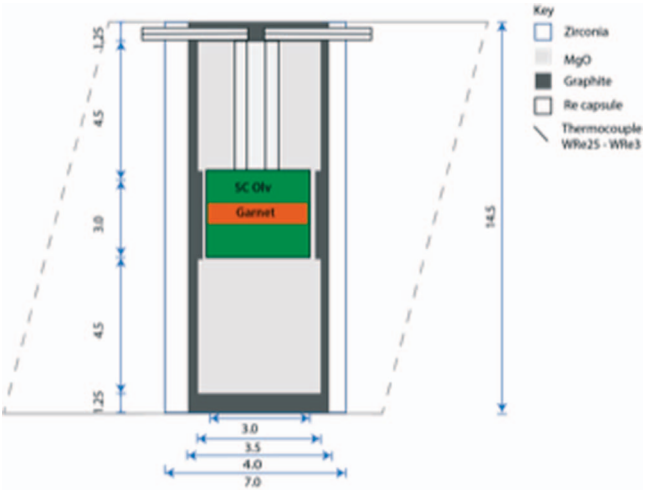

Fig. 1. Schematic cell design of 18/11 multi-anvil assembly used for high-pressure experiments. Double polished garnet slices were sandwiched between San Carlos olivine powder as shown.

Table 1: Chemical composition of experimental starting materials, Bohemia garnet and San Carlos olivine.

	Bohemia Pyrope Garnet	San Carlos Olivine
SiO_2	42.68	41.17
TiO_2	0.57	0.00
Al_2O_3	21.61	0.08
Cr_2O_3	1.52	0.14
FeO	9.15	10.26
MgO	20.82	48.70
Na_2O	0.06	0.00
K_2O	0.00	0.02
CaO	4.37	0.11
Total	10078	10047

Chemical compositions (in wt.%) determined by wavelength dispersive spectroscopy (WDS), at University of Bristol.

METHODS

Experimental techniques

Natural gem pyrope garnets from the Bohemian massif were cut into 200-μm thick slices, using a diamond annular saw, and subsequently double polished to a 0.3-μm diamond finish. Polycrystalline olivine aggregate was formed from optically clean San Carlos olivine, ground to a powder of <1-μm grain size under isopropanol using a McCrone mill. Prior to loading experiments, all starting materials and furnace components were dried overnight at 110°C. The polished garnet slices were embedded into the olivine powder, such that their polished surfaces were oriented perpendicular to the long axis of the cylindrical capsule, which was constructed of double wrapped 25-μm thick rhenium foil (Fig. 1). The composition of starting materials, as determined by electron probe micro-analysis, are presented in Table 1.

Table 2: Experimental conditions and run products

Experimental run	T (°C)	Pressure (kbar)	Time (h)	Phases present	Reaction products	Reaction rim (μm)
E17–012	1000	10	12	Grt, Olv		
E16–073 ◇	1000	13	6	Grt, Olv		
E16–035 ◇	1000	14	12	Grt, Olv		
G18–004 [a] ◇	1000[b]	10	168	Grt, Olv, Opx, Sp, An	Opx, Sp, An	
E17–050	1050	10	6	Grt, Olv, Opx, Sp, Melt	Opx, Sp, An	14.6 (0.7)
E17–053	1050	10	25	Grt, Olv, Opx, Sp, Melt	Opx, Sp, Sp, Melt	17.3 (1.6)
E17–059	1050	10	48	Grt, Olv, Opx, Sp, An	Opx, Sp, An	
E17–064 ◇	1050	10	96	Grt, Olv, Opx, Sp, An	Opx, Sp An	
E17–016	1100	10	2	Grt, Olv, Opx, Sp, Melt	Opx, Sp, Melt	11.2 (0.92)
E16–085 ◇	1100	10	6	Grt, Olv, Opx, Cpx, Sp, Melt	Opx, Cpx, Sp, Melt	18.6 (1.35)
E16–088	1100	12	6	Grt, Olv, Opx, Cpx, Sp, Melt	Opx, Cpx, Sp, Melt	8.6 (1.56)
E18–035	1100	12	6	Grt, Olv, Opx, Sp, An	Olv, Opx, Sp, An	
E18–042	1100	12	6	Grt, Olv, Opx, Sp, An	Olv, Opx, Sp, An	
E18–003	1100	12	24	Grt, Olv, Opx, Sp, Melt	Opx, Sp, Melt	
E18–023 ◇	1100	12	70	Olv, Opx, Cpx, Sp, Melt	Opx, Cpx, Sp, Melt	
E16–032	1100	13.5	1	Grt, Olv		
E19–008 ◇	1100	13.5	6	Grt, Olv, Opx, Sp, Melt	Opx, Sp, Melt	
A21–056 [c] ◇	1150	10	240	Grt, Olv, Opx, Sp, An, Melt	Opx, Sp, An, Melt	
E16–031	1200	13.5	0.17	Grt, Olv		
E18–041	1200	13.5	3	Grt, Olv, Opx, Cpx, Sp, Melt	Opx, Cpx, Sp, Melt	9.8 (0.95)
E18–040	1200	13.5	6	Grt, Olv, Opx, Cpx, Sp, Melt	Opx, Cpx, Sp, Melt	6.6 (1.94)
E17–013	1200	13.5	9	Grt, Olv, Opx, Sp, Melt	Opx, Sp, Melt	
E16–090 ◇	1200	13.5	18	Grt, Olv, Opx, Cpx Sp, Melt	Opx, Cpx, Sp, Melt	23.8 (1.94)
E19–003	1200	14	6	Olv, Melt*	Melt*	
E19–004 ◇	1200	14	6	Grt, Olv, Opx, Cpx Sp, Melt	Opx, Cpx, Sp, Melt	
E19–005 ◇	1200	15	6	Grt, Olv, Opx, Cpx, Sp	Opx, Cpx, Sp	0.5 (0.5)
E19–006 ◇	1200	17	6	Grt, Olv		
E17–054	1260	12	3	Grt, Olv, Opx, Sp, Melt*	Opx, Sp, Melt*	
E17–045 ◇	1260	12	6	Grt, Olv, Opx, Sp, Melt*	Opx, Sp, Melt*	
E16–052 ◇	1300	13	6	Grt, Olv, Opx, Sp, Melt*	Opx, Sp, Melt*	
E16–060	1300	13.5	1	Grt, Olv, Melt*	Melt*	
E16–061 ◇	1300	13.5	4	Grt, Olv, Opx, Sp, Melt*	Opx, Sp, Melt*	
E17–023	1300	13.5	1.5	Olv, Melt*	Melt*	
E16–028	1400	13.5	3	Grt, Olv, Opx, Sp, Melt*	Opx, Sp, Melt*	
E16–029 ◇	1400	13.5	7	Olv, Melt*	Melt*	

Experimental run conditions and phases present at the end of experimental runs. Experiments are ordered by temperature then experimental pressure. Phases present are (Grt) Garnet, (Olv) Olivine, (Opx) Orthopyroxene, (Cpx) Clinopyroxene (Sp) Spinel, (An) Anorthite and (Melt) transient melt. Melt* refers to equilibrium melting of garnet, this melt extends beyond the original garnet-olivine interface and fails to produce a kelyphitic reaction rim, at temperatures expected to coincide with the garnet lherzolite solidus. Reaction rim thickness is reported for experiments which displayed Zone 1 and Zone 2 reactions, in some cases the sample was accidentally polished through and an accurate measurement of rim thickness could not be made. Values in parenthesis are two standard error on the mean reaction rim with. [a]Piston cylinder experiment, with talc-pyrex assembly, see text for details. [b]Unstable thermocouple within this experiment, temperature error +/− 50°C. [c]Piston cylinder experiment, with CaF_2 assembly. Experiments with ◇ are used within phase diagrams.

High-pressure experiments were conducted in the 1000-tonne-force Walker-type multi-anvil press in the Department of Earth Sciences at University College London (Kawai & Endo, 1970; Walker *et al.*, 1990). An 18/11 cell assembly, with stepped graphite furnace, was used to reach pressures of 12–20 kbar and temperatures between 1000°C and 1400°C. Type-D W-Re (3–25%) thermocouples were placed axially along the furnace with the hot junction in contact with the garnet bearing capsule to monitor temperature (Fig. 1). Pressure was calibrated using room temperature transitions of Bi and the high-*T* phase transitions in SiO_2 (quartz–coesite) and $CaGeO_3$ (garnet–perovskite), and the spinel to garnet reaction for our composition of starting materials. The estimated uncertainties in reported pressures are 1 kbar.

Additional piston cylinder experiments were conducted at University College London, and Macquarie University using piston cylinder apparatus. Standard ½" talc–pyrex assemblies were used at University College London with, graphite furnaces and Type-D W-Re (3–25%) thermocouples to monitor temperature. Experiments performed at Macquarie University used a rapid quench end-loaded piston cylinder apparatus with a ½" assembly of natural CaF_2. Temperature was monitored with Type-B $Pt_{30}Rh_{70}$–Pt_6Rh_{94} thermocouples and pressure calibrations were conducted using the quartz-coesite transition (Perrillat *et al.*, 2003) and the albite = jadeite + quartz reaction (Holland, 1980).

All experiments were performed by first compressing the assembly to the desired load, normally over 1–2 hours, prior to increasing the temperature over 30 minutes. Run durations at high-temperature ranged between 1 hour and 10 days, and span the *PT* conditions of the spinel lherzolite stability field (Table 2). Experiments were completed by turning off the furnace power to rapidly quench to room-temperature (taking <10 s to reach temperatures below 100°C) followed by slow decompression, over at least 12 hours, to minimise decompression cracks within reaction rims.

Analytical techniques

Upon recovery samples were mounted in epoxy resin, sectioned parallel to the furnace axis until the garnet became exposed and further polished to a 0.3-μm diamond finish. The sectioning geometry ensured that garnets were exposed perpendicular to

Table 3: Representative major element chemical compositions of garnet

Garnet	E17–012	E16–073	E17–016	E18–042	E17–013	E16–090	E16–085
n	6	8	5	10	4	4	3
SiO_2	43.11	42.90	42.53	42.74	42.89	43.02	41.93
TiO_2	0.55	0.55	0.54	0.45	0.29	0.51	0.57
Al_2O_3	21.91	21.50	21.38	22.21	23.24	21.69	21.20
Cr_2O_3	1.52	1.58	1.57	1.57	1.14	1.74	1.52
FeO	8.55	8.81	8.47	8.08	6.91	8.84	8.68
MnO	-	-	-	0.31	-	-	-
MgO	21.12	20.80	20.94	21.31	21.72	20.99	20.64
CaO	4.42	4.39	4.43	4.41	3.80	4.41	4.39
Na_2O	0.07	0.07	0.06	0.07	0.01	0.08	0.05
K_2O	0.00	0.00	0.01	0.00	0.01	0.00	0.00
TOTAL	101.26	100.60	99.93	101.15	100.00	101.29	98.98
Si	3.02	3.02	3.03	3.00	3.01	3.02	3.02
Ti	0.03	0.03	0.03	0.02	0.02	0.03	0.03
Al	1.81	1.82	1.79	1.84	1.92	1.80	1.80
Cr	0.08	0.08	0.09	0.09	0.06	0.10	0.09
Fe	0.50	0.50	0.50	0.47	0.41	0.52	0.52
Mn	0.00	0.00	0.00	0.02	0.00	0.00	0.00
Mg	2.21	2.21	2.22	2.23	2.27	2.20	2.21
Ca	0.33	0.33	0.34	0.33	0.29	0.33	0.34
Na	0.01	0.01	0.01	0.01	0.00	0.01	0.01
K	0.00	0.00	0.00	0.00	0.00	0.00	0.00
$\sum$	8.00	8.01	8.01	8.02	7.98	8.01	8.01
Py	0.74	0.74	0.74	0.74	0.76	0.73	0.74
Al	0.17	0.17	0.17	0.16	0.14	0.17	0.17
Gr	0.11	0.11	0.11	0.11	0.10	0.11	0.11

Oxides in wt.%, cations per 12 oxygen atoms.

their originally polished surfaces. Carbon-coated samples were imaged using a JEOL JSM-6480LV scanning electron microscope (SEM) in back scattered electron imaging (BSE) mode, operated at an accelerating voltage of 15 kV and 10-nA current. Mineral phases of spinel, orthopyroxene and clinopyroxene were identified using SEM-BSE imaging in combination with energy-dispersive spectroscopy (EDS). Once all phases had been assigned melt was noticeable as a quenched glass with edges which noticeably embayed contacts with the garnet, EDS qualitatively confirmed the presence of a melt phase.

Mineral chemistry was quantified using wavelength-dispersive spectroscopy (WDS) at Birkbeck, University of London using a 3-spectrometer JEOL JXA8100 superprobe, operating at 15-kV accelerating voltage with a beam current of 10 to 25 nA, using three crystals (TAP, LIF and PET) and a Φ (ρz) correction. The electron microprobe was calibrated using typical silicate and oxide standards before use for silicate minerals with an interest in major elements only. WDS measurements were taken by pre-programming positions of interest and running overnight analyses to collect spectra. Two setups were used with varying beam current and spot size: the first setup was used for collecting spectra of garnet, olivine, pyroxenes and spinel, with a 25 nA current, focused beam (0 μm nominal spot size), and acquisition to background time of 40/20 s, respectively. The second setup was required for delicate silicate glasses (melt) and feldspar, which are prone to beam damage. To minimise damage the beam was defocused to a 5-μm spot size and current reduced to 10 nA; collection times were also reduced to 20/10-s acquisition to background time, respectively. A third setup was used to nominally estimate the chemical composition of fine-grained intergrowths represented by more than one phase. This setup analysed the 'bulk' compositon of kelyphite by the use of a defocused 20-μm beam over a 50-μm^2 area for comparison to the parent pyrope garnet.

Some mineral chemistry data were acquired at the University of Bristol using a Field Emission Electron Probe Analyser (FE-EMPA) JEOL JXA8530F, with five spectrometers. The same operating conditions, as described above, were used for WDS measurements collected at the University of Bristol. Mineral chemistries are reported in Tables 3-8.

Electron backscattered diffraction (EBSD) was undertaken at Liverpool University using a CamScan X500 CrystalProbe field emission gun scanning electron microscope (FE-SEM), operating at 20-kV accelerating voltage, 35-nA beam current, working distance of 25 mm and step size of 0.1 μm. EBSP's were automatically indexed using the Oxford Instrument's HKL CHANNEL 5 software package.

In some samples, mineral size permitting, water contents were estimated using the Nicolet iN10 infrared (FTIR) microscope at University College London. Samples were double polished to 75- to 100-μm thickness, olivine and garnet were targeted for water content estimation. Unpolarized infrared absorption spectra were obtained from an aperture area of 25 × 25 μm.

RESULTS

Reaction products and textures

The terminology of coronae surrounding garnet can be confusing; classifications are variously based on textures, mineralogy and/or

Table 4: Representative major element compositions of olivine

Olivine	E17–012	E16–073	E17–016	E18–042	E16–090	E16–085
n	4	6	3	9	2	4
SiO_2	43.31	40.69	41.05	40.66	41.67	40.18
TiO_2	0.02	0.02	0.01	0.09	0.02	0.04
Al_2O_3	0.86	0.25	0.32	3.06	0.07	0.30
Cr_2O_3	0.06	0.05	0.04	0.31	0.22	0.07
FeO	9.56	10.21	10.24	11.12	9.45	10.84
MnO	-	-	-	0.30	-	-
MgO	46.01	47.25	47.36	43.94	50.28	47.80
CaO	0.36	0.20	0.22	0.75	0.15	0.31
Na_2O	0.02	0.02	0.01	0.08	0.00	0.01
K_2O	0.01	0.03	0.01	0.00	0.01	0.02
TOTAL	100.21	98.73	99.26	100.31	101.87	99.57
Si	1.05	1.01	1.01	1.00	1.00	0.99
Ti	0.00	0.00	0.00	0.00	0.00	0.00
Al	0.02	0.01	0.01	0.09	0.00	0.01
Cr	0.00	0.00	0.00	0.01	0.00	0.00
Fe	0.19	0.21	0.21	0.23	0.19	0.22
Mn	0.00	0.00	0.00	0.01	0.00	0.00
Mg	1.66	1.75	1.74	1.61	1.80	1.76
Ca	0.01	0.01	0.01	0.02	0.00	0.01
Na	0.00	0.00	0.00	0.00	0.00	0.00
K	0.00	0.00	0.00	0.00	0.00	0.00
$\sum$	2.94	2.99	2.98	2.96	3.00	3.00
Mg#	89.56	89.19	89.19	87.57	90.46	88.71

Oxides in wt.%, cations per 4 oxygen atoms.

Table 5: Representative major element compositions of spinel

Spinel	E17–016	E18–042	E17–013	E16–090	E16–085
n	3	4	1	3	4
SiO_2	0.19	0.51	2.20	0.49	0.50
TiO_2	0.13	0.26	0.16	0.15	0.25
Al_2O_3	61.67	60.12	58.49	57.31	60.11
Cr_2O_3	6.37	8.73	8.44	11.94	8.73
FeO	8.82	9.52	7.96	7.45	9.52
MnO	-	-	-	-	0.20
MgO	21.28	21.07	21.82	22.39	21.06
CaO	0.08	0.06	0.04	0.08	0.05
Na_2O	0.00	0.01	0.01	0.00	0.01
K_2O	0.00	0.00	0.00	0.01	0.00
TOTAL	98.53	100.27	99.12	99.81	100.47
Si	0.00	0.01	0.06	0.01	0.01
Ti	0.00	0.00	0.00	0.00	0.01
Al	1.86	1.80	1.75	1.73	1.90
Cr	0.13	0.18	0.17	0.24	0.19
Fe	0.19	0.20	0.17	0.16	0.21
Mg	0.81	0.80	0.83	0.85	0.01
Ca	0.00	0.00	0.00	0.00	0.61
Na	0.00	0.00	0.00	0.00	0.00
$\sum$	3.00	3.00	2.98	3.00	2.94
Cr#	6.48	8.88	8.83	12.26	8.88
Mg#	81.14	79.78	83.01	84.27	79.78

Oxides in wt.%, cations per 4 oxygen atoms.

the reactions speculated to have formed the corona. Here, the term kelyphite will be used generally to describe any form of corona, or reaction rim, surrounding garnet.

Many of the experimentally reproduced textures in this study fit the terminology introduced by Obata & Ozawa (2011), including 'coarse opx rim' (COR), 'nodular spinel', and 'unconformity structures'. For a complete description of terminology in relation to breakdown reactions, the reader is referred to Obata & Ozawa (2011). These terms will be used to describe similar textures identified in this study to limit the confusion caused by new terminology.

Before proceeding with a complete description of the various observed kelyphite textures, we highlight the ubiquitous presence of a melt phase, which was observed in most 'high-temperature' (above 1000°C) reaction products. This melt phase is interpreted to be a disequilibrium melt formed by the incongruent melting of garnet during breakdown as has been described in natural samples by Hunter & Taylor (1982). The melts origin and possible metastability are discussed in detail after the description of experimental results.

Representative images of recovered samples are shown in Figs 2–12, experimental results are presented in Table 2, and reaction product as well as relic olivine and garnet compositions are presented in Tables 3–8. The experimental results are plotted with respect to thermodynamically calculated garnet lherzolite pseudosections in Figs 13–15. Experimental kelyphites, produced between the spinel lherzolite solidus and 1000°C, show at least three concentric zones following garnet breakdown. Each zone has different mineralogy and textures and is numbered sequentially inwards from the interface with olivine.

Zone 1 is a coarse-grained granular orthopyroxene with grain sizes larger than 5 μm. Small, ~2-μm, euhedral spinel grains delineate the original garnet-olivine boundary (Figs 2, 3 and 4). The thickness of this outermost shell varies with temperature, and it is most developed at temperatures of 1200°C (Fig. 4a and b).

Table 6: Representative major element compositions of pyroxenes

	Orthopyroxene				Clinopyroxene
	E17–016	E17–013	E16–090	E16–085	E16–085
n	4	4	3	2	1
SiO_2	52.43	51.77	52.86	51.00	50.00
TiO_2	0.21	0.25	0.22	0.33	0.48
Al_2O_3	9.10	9.68	8.50	9.62	8.39
Cr_2O_3	0.65	0.54	0.98	0.60	0.62
FeO	6.73	6.52	6.63	7.78	5.78
MgO	30.39	29.40	30.98	28.13	19.00
CaO	1.19	1.50	1.04	2.23	14.79
Na_2O	0.06	0.06	0.08	0.06	0.20
K_2O	0.00	0.00	0.00	0.01	0.02
TOTAL	100.78	99.73	101.27	99.78	99.28
Si	1.80	1.80	1.81	1.79	1.81
Ti	0.01	0.01	0.01	0.01	0.01
Al	0.37	0.40	0.34	0.40	0.36
Cr	0.02	0.01	0.03	0.02	0.02
Fe	0.19	0.19	0.19	0.23	0.18
Mg	1.56	1.52	1.58	1.47	1.03
Ca	0.04	0.06	0.04	0.08	0.57
Na	0.00	0.00	0.01	0.00	0.01
$\sum$	4.00	3.99	4.00	4.00	3.99
Cr#	4.58	3.64	7.15	4.00	4.71
Mg#	88.94	88.93	89.29	86.56	85.42
Wo	2.45	3.15	2.11	4.70	32.34
En	86.76	86.13	87.40	82.49	57.79
Fs	10.79	10.72	10.49	12.81	9.87

Oxides wt.%, cations per 6 oxygen atoms.

Table 7: Representative major element compositions of feldspar

Feldspar	E18–042	E18–042
SiO_2	58.61	53.98
TiO_2	0.00	0.12
Al_2O_3	26.13	22.94
Cr_2O_3	0.04	0.00
FeO	0.28	2.77
MnO	0.04	0.05
MgO	0.06	8.87
CaO	7.78	6.24
Na_2O	7.44	5.84
K_2O	0.14	0.00
TOTAL	10052	10081
Si	2.61	2.44
Ti	0.00	0.00
Al	1.37	1.22
Cr	0.00	0.00
Fe	0.01	0.10
Mn	0.00	0.00
Mg	0.00	0.60
Ca	0.37	0.30
Na	0.64	0.51
K	0.01	0.00
$\sum$	5.02	5.19
An	53.31	54.15
Ab	46.13	45.85

Oxides in wt.%, cations per 8 oxygen atoms.

Table 8: Representative major element compositions of transient melt

Transient melt	E17–016	E16–085
n	8	6
SiO_2	36.36	44.21
TiO_2	0.96	1.14
Al_2O_3	17.57	19.73
Cr_2O_3	0.13	0.13
FeO	6.70	6.80
MgO	9.49	7.14
CaO	11.00	11.96
Na_2O	2.03	1.07
K_2O	0.72	0.38
TOTAL	84.96	92.56
Si	3.14	3.42
Ti	0.06	0.07
Al	1.79	1.80
Cr	0.01	0.01
Fe	0.48	0.44
Mg	1.22	0.82
Ca	1.02	0.99
Na	0.34	0.16
$\sum$	8.07	7.70

Oxides in wt.%, cations per 12 oxygen atoms. Garnet stoichiometry assumed.

This zone extends into the olivine beyond the original garnet–olivine boundary. Similar outer shells have previously been termed 'coarse orthopyroxene rims' (COR) by Obata & Ozawa (2011) (Figs 2 and 3, b and d). Nodular spinel nucleation appears to occur along the original garnet–olivine interface, as observed in natural kelyphites (Obata & Ozawa, 2011; Špaček *et al.*, 2013). Nodular spinel appears isolated, surrounded by the COR. In some cases, additional spinel grains are elongated perpendicular to the original garnet-olivine interface, growing towards the garnet interior (Fig. 2). As spinel grows towards the interior of the garnet, its crystal habit becomes subhedral and elongated (Fig. 3b).

Zone 2 is a coarse-grained, ~10–20-μm, intergrowth of spinel in an orthopyroxene matrix, with occasional clinopyroxene. Also present is a small amount of melt contained between the crystallising spinel/orthopyroxene and the retreating garnet (Figs 3 and 4). The melt occurs within, and never beyond, the boundaries of the original garnet (Fig. 4a–e). Small pockets of melt are occasionally observed on the grain boundaries of the solid reaction products (Fig. 4d). The spinel and pyroxene appear to grow towards the retreating garnet interface and into the melt, as also observed by Hunter & Taylor (1982).

The reaction products of spinel and pyroxene appear to have crystallised from the melt. Both spinel and pyroxenes have straight facetted interfaces with the melt, whereas garnet has irregular, embayed, interfaces with the melt, consistent with dissolution of garnet and growth of pyroxene and spinel (Fig. 4d). As garnet breakdown progresses, following the melt development, garnet continues to melt at its edge and the solid products grow as an irregular facetted rim into the melt. Eventually all the garnet and melt are consumed, leaving a coarse-grained intergrowth of spinel and pyroxenes, surrounded by a rim of COR and nodular spinel as the final pseudomorph replacing the original garnet (Fig. 2c and d).

Zone 3 ; a fine-grained lamellar intergrowth of olivine, spinel and plagioclase feldspar (Fig. 5) (characterised by EBSD analysis, Fig. 5b) is observed at 1100°C and 12 kbar. This kelyphite is similar the 'metasomatic kelyphite' described by Obata *et al.* (2014).

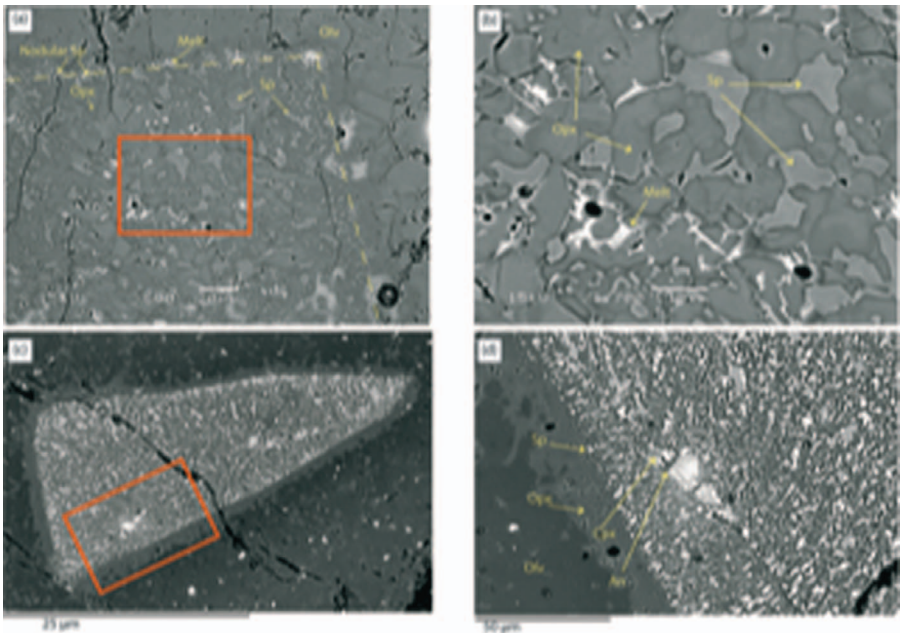

Fig. 2. SEM micrographs of complete garnet breakdown, there is no visible garnet left but small pockets of melt are present between the solid reaction products of spinel and orthopyroxene. (a) E18–023, 1100°C, 12 kbar, 70 hrs. The position of garnet is marked by nodular spinel and the COR. (b) A magnified image of the region highlighted by the red box. A coarse grained intergrowth is replacing the initially fine grained texture of spinel and orthopyroxene. Minor melt is visible at grain boundaries between minerals, which is being consumed by their growth. (c) A21–056, 10 kbar, 240 hours. There is no garnet left in this experiment with complete reaction to spinel, orthopyroxene and clinopyroxene. An outer coarse orthopyroxene rim is clearly visible. (d) A magnified image of the region highlighted by the red box in (a), a fine grain intergrowth texture is present throughout the former garnet. Infrequent tiny patches of melt are present near the garnet edge; the interior is completely reacted with no present.

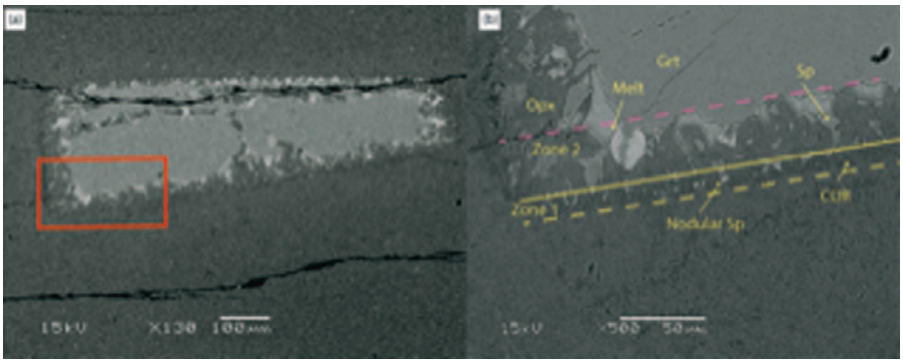

Fig. 3. SEM micrograph of experiment E16–085, 1100°C, 10 kbar, 6 hours. (b) is a magnified image of the red box in (a). Sp, spinel, Grt, garnet, Opx, orthopyroxene, Melt. Garnet breakdown appears to follow a characteristic breakdown sequence, beginning with the formation of a coarse orthopyroxene rim (COR), which extends beyond the garnet-olivine interface. Followed by, nodular spinel which delineate the original garnet-olivine boundary, then clinopyroxene nucleates (dependent on the initial garnet chemistry), and finally the melt phase forms following an established COR and nodular spinel growth. Zones 1 and 2 are shown in (b), nodular spinel and the coarse orthopyroxene rim (COR) constitute Zone 1. Whereas Zone 2, includes matrix opx, elongated spinel and melt.

Textures in this zone of 'metasomatic type' kelyphite can be subdivided into two distinct sub-regions; an outer coarse-grained rim (Zone 3a) (~ 10 micrometre) of alternating olivine and spinel with occasional orthopyroxene and an inner region (Zone 3b) consisting of spinel, olivine and plagioclase feldspar. The inner rim is characterised by a network of fibrous interconnected lamellae, similar to textures seen following breakdown of a single phase. Olivine and anorthite appear as adjacent vermicular interconnected strings, with isolated spinel along edges (Fig. 5c). Large anorthite crystals separate the outer region (Zone 3a) from the lamellar internal structure (Zone 3b).

Zone 3b kelyphite grow inward towards the retrogressing garnet and 'unconformity' structures can be observed most easily at junctions between spinel grains, where their growth direction abruptly changes (Obata, 2011).

The fine-grained nature of the internal kelyphite prevents detailed chemical compositions being measured. Previous studies concluded this type of kelyphite resulted from interactions with a fluid phase (Obata *et al.*, 2014). However, experiments in this study did not possess free fluids and no melts were observed in these experiments (E18-003 and E18-042). Faceted spinel and olivine grains surrounding the lamellar internal kelyphite might, however, provide evidence of melt involvement in the reaction. So, while a melt is not found in this lamellar layer, given the observations in Zones 1 and 2 it is likely involved in the crystallisation of this kelyphite (Fig. 5).

Zone 4; the final kelyphite texture observed within these experiments occurred only at temperatures lower than 1150°C, and at pressures equal to 10 kbar. Recovered samples show fine-grained lamellae, consisting of orthopyroxene, spinel and plagio-

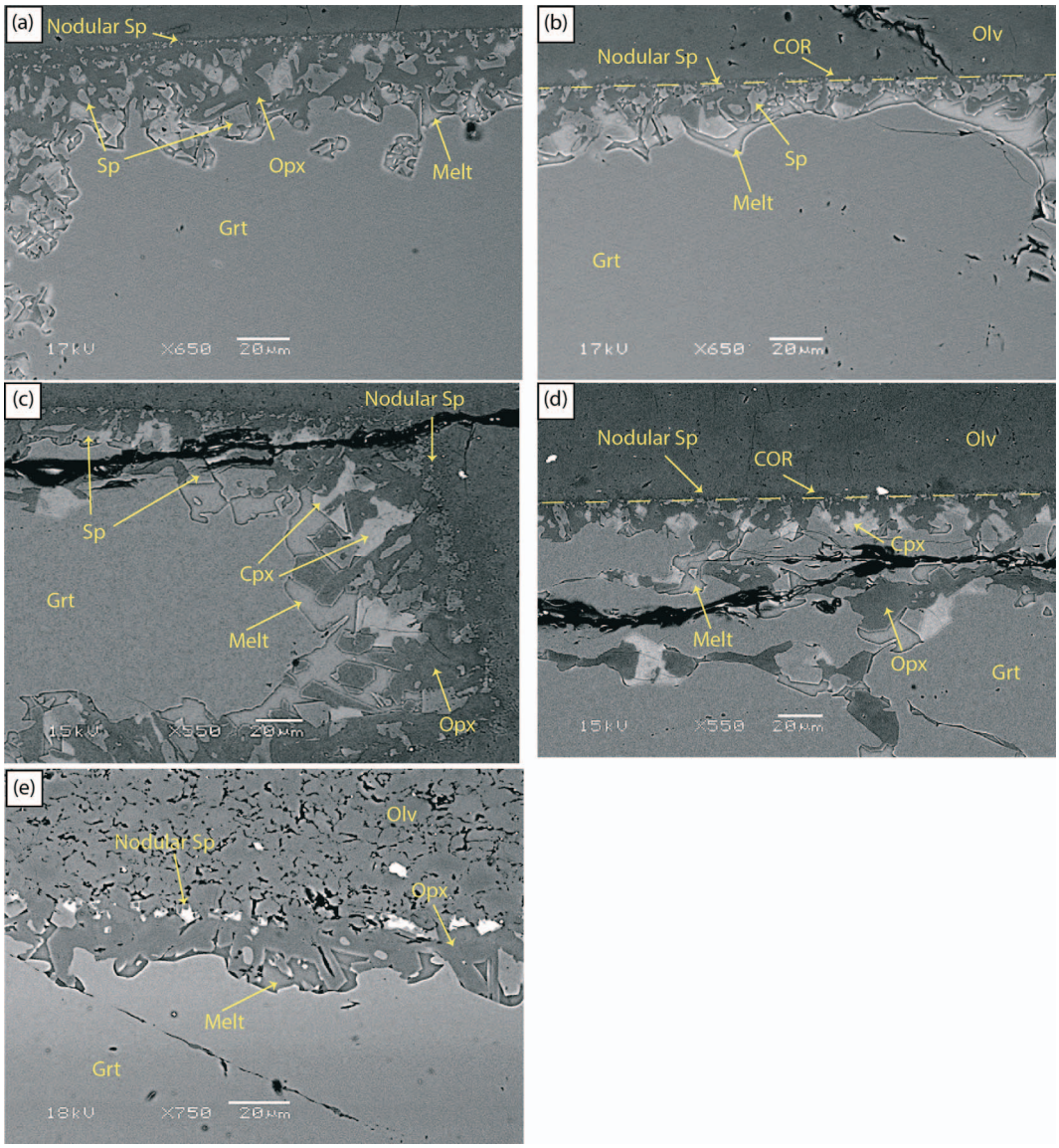

Fig. 4. Example SEM images of the textures produced by garnet breakdown. (a and b) E18–041, 1200°C, 13.5 kbar, 3 hours. Images (a) and (b) show the full length of the reaction rim on the experimental garnet. Nodular spinel clearly delineate the original garnet–olivine boundary, enclosed with a COR, with melt occupying the region between garnet regression and COR growth. (c) E16–085, 1100°C, 10 kbar, 6 hours. As in nature, the reaction rim grows inward towards the retrogressing garnet and on average rim thickness is constant. (d) A magnified image of E16–085, ortho- and clinopyroxene grow into pockets of melt formed along fractures within the interior of garnet. Overall the replacement of garnet is through solid phases, with minor melt in isolated pockets. (e) E17–016, 1100°C, 10 kbar, 2 hours. The earliest stages of garnet breakdown, with a poorly formed COR, bright chromium rich nodular spinel and small melt pockets.

clase feldspar. Some Zone 4 kelyphite is surrounded by a poorly developed rim of Zone 1. (Figs 6, 7 and 8).

In some recovered samples (E17-059) a transition from the concentrically zoned kelyphite intergrowth, Zones 1–2, to a melt free fine-grained kelyphite (Zone 4) observed at constant *PT* conditions. This contains spinel, orthopyroxene and anorthite, consistent with direct breakdown of the garnet without the olivine component, Equation 2 (Fig. 6).

The bulk composition of the Zone 4 kelyphite was determined (Table 9) and its constituent phases identified by chemical mapping and electron backscattered diffraction (EBSD) (Figs 6, 7 and 8, and Table 9). The Zone 4 kelyphite typically show a poorly developed COR at their outer edges, and those produced in the experiments at durations less than 48 hours at 1050°C also contain frozen melt pockets, but no internal isochemical kelyphite. The COR rims from these short duration experiments were indistinguishable from those developed at higher temperatures. At durations greater than 48 hours, fine-grained (< 1 μm) fibrous intergrowths develop between the garnet and an already existing COR, appearing to replace garnet without the involvement of a melt. As with other eutectoid breakdown reactions, the kelyphite grew in domains, similar to descriptions from Obata & Ozawa (2011), where the growth direction is indicated by the orientation of sub-parallel lamellae of alternating spinel, orthopyroxene and feldspar (Fig. 8a), and verified by EBSD mapping (Fig. 9). Growth domains demonstrate nucleation of the kelyphite occurred at the outer edges of, or fractures within, garnet, contrasting with Zone 3 intergrowths that nucleate within garnet interiors (Fig. 5c).

At temperatures of 1000°C (or lower) and durations less than 168 hours no reaction was observed in any experiments at pressures of 10–14 kbar. Recovered samples show decompression fractures along a very straight garnet–olivine interface (Fig. 10) and in

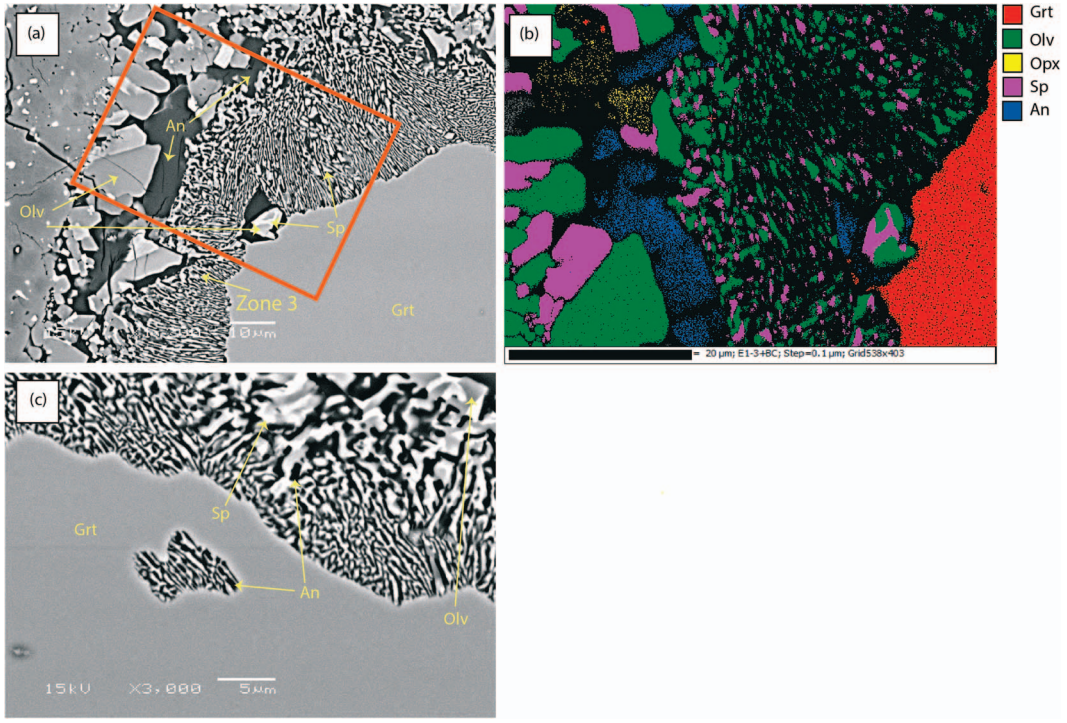

Fig. 5. A metasomatic kelyphite (Zone 3) was observed at temperatures of 1100°C and 12 kbar. This kelyphite is composed of olivine, spinel and anorthite with minor orthopyroxene outside of the COR. There is no evidence of the melt phase being present within this type of kelyphite. (a) E18–035, 1100°C, 12 kbar, 6 hours. The lamellae texture is common with kelyphite and is a fine grained intergrowth of olivine and spinel (brightest features in the micrographs), with anorthite which appears as black in the above SEM micrograph. Phases were identified by electron back scattered diffraction (EBSD) at the University of Liverpool. (b) An EBSD map of the red highlighted region in (a). (c) A magnified image of the kelyphite structure, with an internally nucleated kelyphite. This small internal kelyphite may have nucleated on a defect present within garnet.

Table 9: Composition of starting garnet and kelyphite

	Garnet	Zone 4 kelyphite	σ
SiO2	41.64	41.08	0.24
TiO2	0.39	0.45	0.02
Al2O3	21.99	22.98	0.13
Cr2O3	1.56	0.01	0.01
FeO	8.07	12.07	0.15
MnO	0.35	0.36	0.14
MgO	21.07	17.42	0.11
CaO	4.42	5.10	0.01
NiO	0.01	0.01	0.02
Na2O	0.08	0.07	0.01
Total	99.57	99.54	

Average bulk WDS (wt.%) composition of kelyphite, analysed by a defocused 20 μm beam over a 50 μm^2 area for comparison to pyrope garnet. Standard deviation calculated from 22 spot analyses. Close correspondence between kelyphite bulk composition and original Bohemia garnet suggests breakdown of garnet via Reaction 2. FeO and Cr_2O_3 show the greatest variation between the kelyphite and parent garnet can be accounted for by unsampled spinel which too small to be analysed by the defocused beam.

some cases the garnet–olivine interface became rough compared to the initial surface polish, and decompression fractures did not follow this interface (Fig. 11a), suggesting the very beginnings of a reaction. Experiment G18-004 produced a melt-free kelyphite with a large proportion of the original garnet still present even after 168 hours at high temperature (Fig. 12).

Quenched glasses

Evidence of the presence of melt (i.e. quenched glass) is observed in almost all high temperature (above 1000°C) experiments, conducted as part of this study. The melt is confined to the region between the retrogressing garnet and growing spinel and pyroxenes, as observed by Hunter & Taylor (1982). The reaction products (spinel + pyroxene) grow as euhedral faceted grains (Fig. 4), consistent with unimpeded growth into a melt. In experiments where garnet is entirely consumed and replaced by spinel + pyroxenes, residual melt pockets are found at the grain boundaries and triple junctions of the reaction products (Fig. 2a and b).

Based on the location, volumetric extent and textures of the observed melt, along with the fact that it is consumed as the reaction progresses, we believe it is a transient phase during garnet breakdown, appearing to only catalyse breakdown but not modify the final equilibrium assemblage (Hunter & Taylor, 1982). While the melt is consumed during complete garnet breakdown (Fig. 2c and d), its presence enhances chemical mobilities, assisting in diffusive transport of nutrients to the newly growing reaction products. The presence of melt appears to be an essential catalyst for the retrogression process of garnet in the presence of olivine, following Reaction 1, at least within the parameters of experiments in this study.

FTIR reveals the presence of small quantities of OH associated with grain boundaries (identified by diffuse broad signal) and within the remnant garnet portions likely hosted in the melt (Supplementary Fig. 2). While it is not feasible to quantify the experimental water content, the observed switch in garnet breakdown mechanism and onset of melting cannot be attributed to experiments being totally anhydrous.

In an attempt to define the pressure–temperature space where a change from melt assisted breakdown to solid-state breakdown occurs, and demonstrate the transient nature of the melt, multiple additional long duration (168 and 240 hours) experiments were conducted at 10 kbar and ~1000°C (G18-004) and 10 kbar at 1150°C

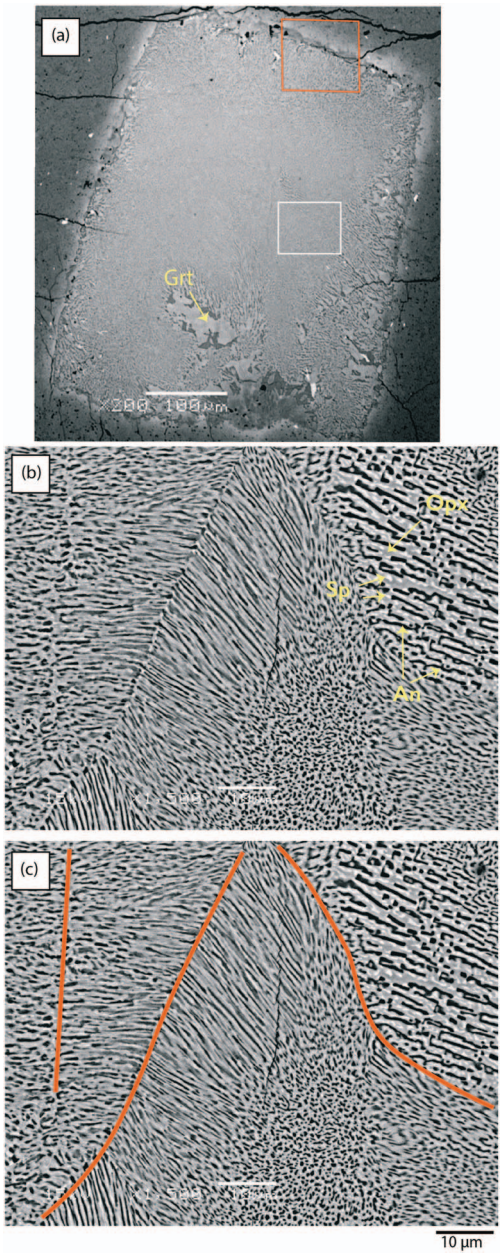

Fig. 6. An example of kelyphite resulting from Reaction 2 (Zone 4). (a) E17–059, 1050°C, 10 kbar, 48 hours. Nearly the entire garnet is replaced by fine grained lamellae of spinel, anorthite and orthopyroxene. The kelyphite is surrounded by the COR. (b) A magnified image of the white box. The unconformity structures are clearly visible as straight lineation's through the kelyphite. Orthopyroxene appears as massive strings, with isolate pulled spinel sitting within it. Anorthite also forms long strings, visible as the black regions. (c) Unconformity structures have been highlighted from (b); these form due to curvature in the garnet. Each unconformity divides kelyphite domains as discussed by Obata (2011).

(A21-056). Experiment G18-004 showed no evidence of a COR (Zone 1) and instead breakdown proceeded by direct breakdown of garnet to an assemblage of spinel + orthopyroxene + anorthite (Fig. 12). At this low temperature, without a melt, the rate of garnet breakdown is clearly reduced, as even after 168 hours at temperature a large volume of the garnet remained unreacted. The failure to produce even a poorly developed COR implies olivine was not consumed in this reaction, even during the earliest stages of garnet breakdown. At higher temperatures and the same pressure (A21-056, 1150°C, Fig. 2c and d) garnet breakdown proceeded with olivine as a reactant phase resulting in the development of a large COR, nodular spinel, clinopyroxene and anorthite as reaction products. EDS mapping confirmed the presence of a single isolated melt pocket within the COR; no further melt was present within the internal kelyphite and the garnet had been completely consumed (Fig. 2c and d). Experiment A21-056 confirmed that over long durations at high temperatures (above 1000°C) any melts present would be consumed during the growth of reaction products. This experiment also differs from those that produced a Zone 3 'metasomatic-type kelyphite' as olivine was not identified as a reaction product within the kelyphite structure. Moreover, the internal structure closely resembled Zone 4 textures of complex intergrowths of spinel, anorthite and orthopyroxene, but these are coarser than experiments run at lower temperatures and shorter durations (Fig. 6).

Mass balance and thermodynamic phase equilibria

To constrain the reactions taking place and the role of melting during garnet breakdown, mass balance calculations were performed. As the small melt volume in most experiments precluded accurate chemical analysis, the chemistries recovered from Experiment E17-016 were assumed to be representative of those throughout this study (Table 8). The composition of the quenched melt is similar to the parent pyrope garnet, with small enrichments in incompatible elements, Ti, Ca, Na and K. The compatible major cations (Mg, Fe, Al, Cr and Si) are slightly depleted in the melt with respect to the parent garnet, consistent with the growth of spinel and pyroxene at the olivine-rich side of the reaction front. Mass balance calculations with nine components were performed for fictive bulk compositions with olivine/garnet ratios varying between 0 and 1 reacting to form the observed assemblage of spinel, orthopyroxene and melt in E17-016. For each fictive composition the predicted phase proportions (percentage weight) were calculated over 10 000 Monte Carlo iterations, where a randomly varying uncertainty was added to each oxide component during each iteration. Overall the varying random errors for each oxide form a Gaussian distribution with standard deviation equal to the reported 1σ analytical uncertainty; reported phase proportions are the mean, and the SSE values report the average squared sum of residuals of all calculation cycles. Bulk compositions containing less than 68.4% garnet do not mass balance if the olivine + garnet = sp + opx + melt reaction is assumed. A bulk composition formed from a mathematical combination of 90% garnet and 10% olivine produces the smallest mass balance SSE misfit statistics. Products of the reaction for this composition are calculated to consist of 14% spinel, 59% orthopyroxene and 31% melt. Table 10 displays the results for mass balance calculations with bulk compositions of garnet varying from 70–100%.

Phase equilibria were investigated using Perple_X (Connolly, 2009) and THERMOCALC (Powell *et al.*, 1998). Thermodynamic data from the database of Holland & Powell (2011) were used alongside solution models for garnet lherzolite from Jennings & Holland (2015), Holland *et al.* (2018) and Tomlinson & Holland (2021). Petrogenetic P–T grids were calculated in Perple_X for bulk assemblages consisting 100:0, 90:10 and 10:90 garnet:olivine, as well as a grid for natural-composition KLB-1 peridotite (Figs 13–15). Solution models from Jennings & Holland (2015) were used for bulk assemblages of 10:90 garnet:olivine as the solution model from Holland *et al.* (2018) resulted in an unrealistically wide garnet + spinel peridotite field at low temperatures, which may result

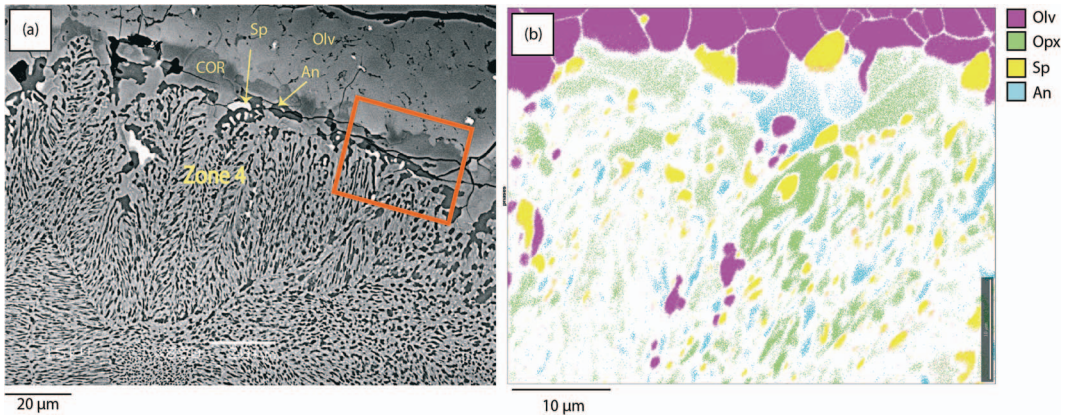

Fig. 7. (a) High magnification image from red box in Fig. 6. Here the COR is clearly visible as the outermost shell in the kelyphite structure. As with the metasomatic kelyphite the international kelyphite is separated by large anorthite grains. The internal structure is clearly follows the expected phase assemblages of spinel + orthopyroxene + anorthite, confirmed by EBSD mapping (b). (b) EBSD map of the region highlighted by the red box. Orthopyroxene grows inward towards the retreating garnet, with spinel nucleating on the edges of orthopyroxene fingers. Anorthite is poorly indexed but visible as the blue lamellae adjacent to the orthopyroxene.

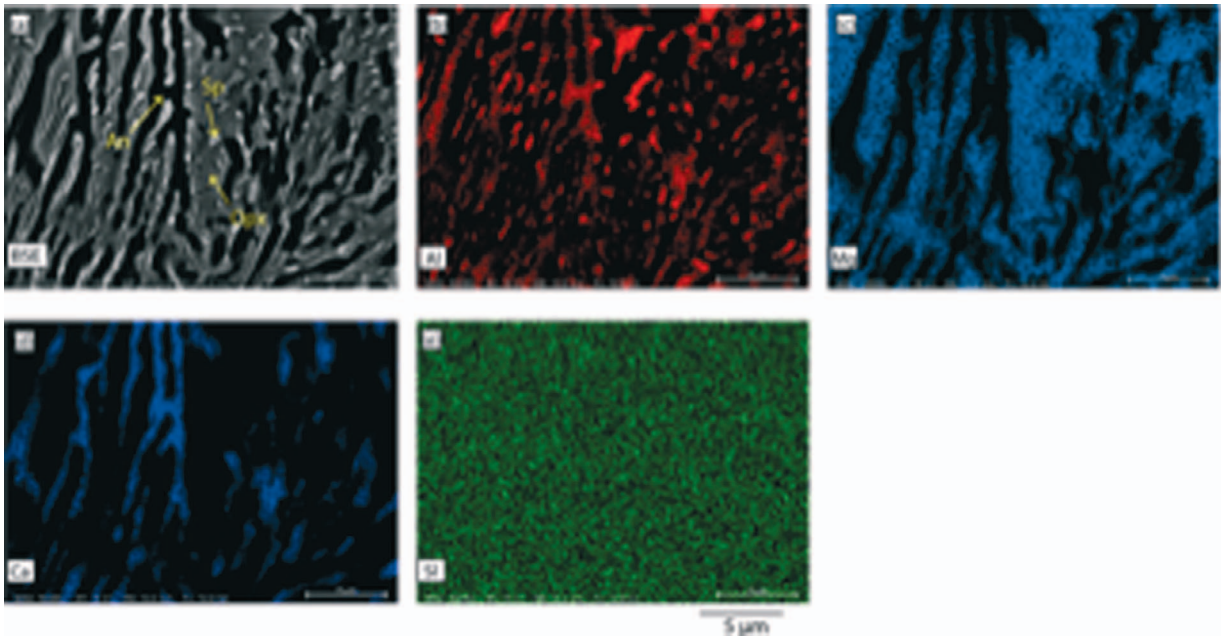

Fig. 8. (a) E17–059 High magnification compositional map of an experimental Zone 4 kelyphite following Reaction 2, there are no detectable melts in experiments. This fine-grained kelyphite results from garnet almost instantaneously nucleating three or four phases, depending on initial chemistry. These form complex vermicular intergrowths with pyroxenes as massive strings and spinel isolated pulled threads inside of these growths, confirmed by EDS chemical maps (b and c) of kelyphite in (a).

Table 10: Results from mass balance calculations, for the reaction of olivine and garnet, to spinel, orthopyroxene and transient melt

Reactants												
Grt	100	98	96	94	92	90	88	86	84	82	80	70
Olv	0	2	4	6	8	10	12	14	16	18	20	30
Products												
Sp	14	14	14	14	14	14	14	14	14	14	14	14
Opx	48	50	52	54	57	59	61	63	65	67	69	80
Transient Melt	45	42	40	37	34	32	29	26	24	21	18	5
r^2	5.78	4.62	3.72	3.07	2.66	2.52	2.63	2.99	3.62	4.47	5.61	15.06

Calculations were performed by varying fictive bulk composition of reactant phases (garnet and olivine), to find percentage volume of products (spinel, orthopyroxene and trainset melt). Bulk compositions with less than 68.4% garnet did not yield products in expected proportions. As garnet content is increased in the bulk composition, transient melt volume increases, at the expense of orthopyroxene. All phases are reported as vol (%). r^2 Values are the average squared sum of residuals of all calculation cycles.

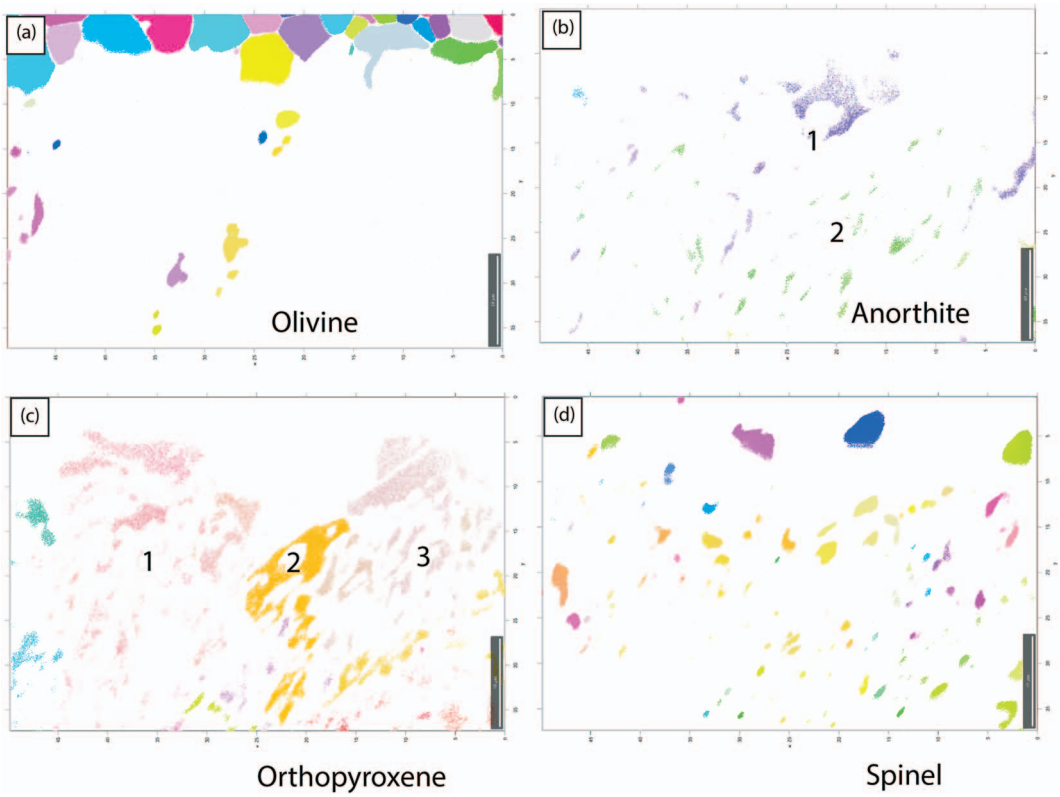

Fig. 9. Orientation maps of experiment E17-059, region highlighted in Fig. 7(a–d) orientation maps of olivine, anorthite, orthopyroxene and spinel. Orthopyroxene shows at least three domains, which may have orientation relationships with spinel, although there is an insufficient number of indexed orientation within spinel to confirm. Anorthite also grows in domains with two visible from the orientation maps; these do not coincide with orthopyroxene domains.

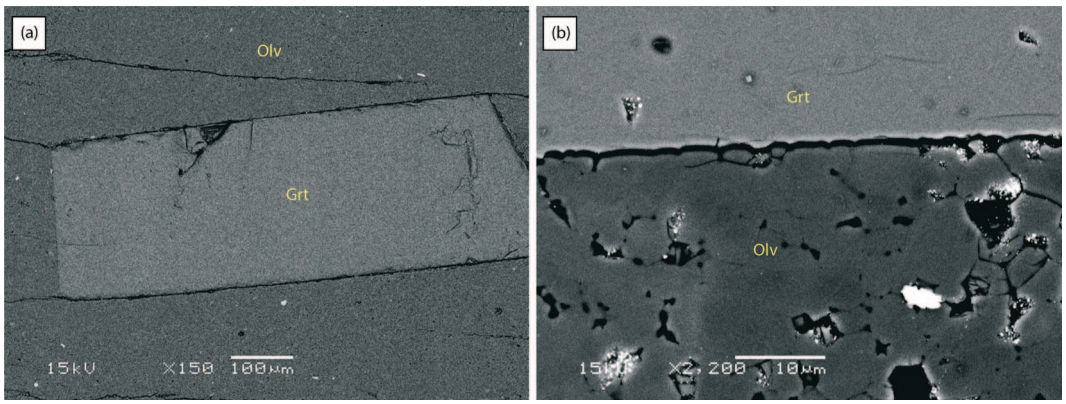

Fig. 10. SEM micrographs of cases where garnet did not react, decompression cracks follow the outline of garnet packed into olivine powder. Decompression cracks did not form along the garnet-olivine boundary once garnet breakdown had begun, mechanically coupling the olivine powder to garnet. (a) E16–073, 1000°C, 13 kbar, 6 hours. (b) E16–032, 1100°C, 13.5 kbar, 1 hour.

from the sensitivity of the solution models to the high chromium content in the bulk composition.

These bulk compositions were chosen to reflect: (i) the calculated mass balance required to form the observed melt (90:10, garnet:olivine – above); (ii) the scenario of a single garnet xenocryst surrounded by olivine (10:90, garnet:olivine; the thermodynamic equilibrium case for the experiments); and (iii) a case relevant to isochemical breakdown of garnet (100:0, garnet:olivine) alongside a natural peridotite bulk composition. In addition, a T–X pseudosection was calculated using THERMOCALC using the peridotite model of Tomlinson & Holland (2021) that is based on the dataset of Holland & Powell (2011), to determine whether melting in our experiments had been induced through a depression in the solidus along a garnet–olivine binary at 12 kbar (Fig. 16).

The position of subsolidus phase boundaries in Figs 13 and 14 are in excellent agreement with experimental results between 1000°C and 1200°C, for garnet breakdown following Reaction 1. However, Fig. 13 a case for 90:10 garne:olivine better reproduces all the observed kelyphite across the experimental results for Zones 1–2. Isochemical breakdown (Reaction 2) is described well by Fig. 15, the case for garnet breakdown in the absence of olivine; however the calculated solidus is at higher temperatures than expected based on observations of melt in our experiments.

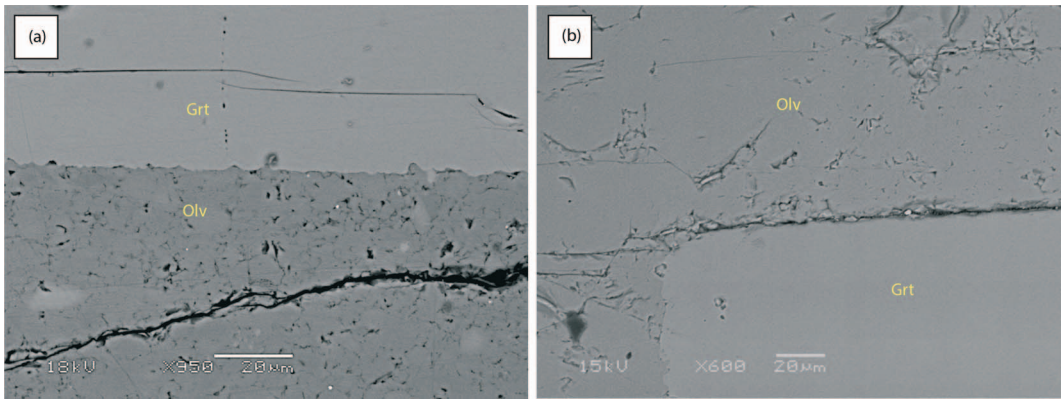

Fig. 11. ow temperature experiments did not produce reaction rims, but there is evidence for the beginnings of garnet breakdown. All garnets were initially polished to ensure a smooth reaction surface in contact with the surrounding olivine. After the experiment the interface between olivine and garnet became wavy and rough. Experiments (a) E17–012, 1000°C, 10 kbar, 12 hours, and (b) E19–006, 1200°C, 17 kbar, 6 hours, show roughening at the garnet-olivine boundary. Given longer to anneal in the spinel stability field these garnets would have reacted following Reactions 1 and 3, respectively.

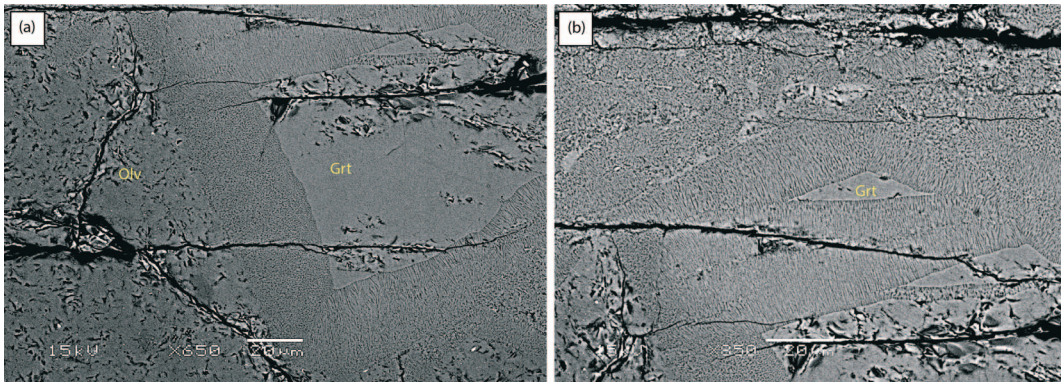

Fig. 12. SEM micrographs of experiment G18–004, 1000°C, 10 kbar. (a) An overview of the remaining garnet enclosed in a very fine grained Zone 4 kelyphite. (b) A magnified image of the kelyphite and a stranded piece of garnet, surrounded by kelyphite. This small segment has unconformity structures at each of its three corners. Suggesting kelyphite grew in three dimensions towards the garnet until encountering another growing front.

The position of the solidus shifts to higher temperatures across a pressure interval of 7–16 kbar, and with the addition of excess olivine in the system (Fig. 14). The calculations predict the spinel lherzolite assemblage transforms to an anorthite-bearing assemblage at pressures of ~10–8.5 kbar. Our experiments appear to echo the predicated phases at each PT interval, across the stability field for spinel lherzolite within experimental PT uncertainties.

Calculated phase equilibria predict that the solidus of the system occurs at 1275–1400°C (1180–1350°C for the calculations of Holland *et al.*, 2018) across the pressure range of the experiments, which is in reasonable agreement with where we observe melt extending beyond the garnet and percolating between olivine grains. Fig. 16 also demonstrates that the position of the equilibrium solidus is ~1320°C and does not predict any low temperature depressions with varying garnet:olivine ratios. The calculated T-X section presented here suggests that melting should not occur at the experimental temperatures and a thermodynamically stable melt phase would not be expected for a wide range of reacting ratios of garnet:olivine from 0:1 to 1:1. A garnet:olivine ratio of 90:10 was determined by mass balance calculations, which falls within the ratios of the calculated T-X section and melts are not predicted at this ratio or ratios which may differ slightly from the mass balance calculations. However, at lower temperatures and above 1050°C, we ubiquitously observe small fraction melts in recovered samples: This melt is required in mass balance calculations of the experimental system, but it is clearly being consumed by the growth of the equilibrium assemblage (Fig. 2c and d).

In the absence of a predicted thermodynamically stable melt, we suggest garnet breakdown is occurring through a disequilibrium mechanism (e.g. Hunter & Taylor, 1982). In which a melt phase acts as a catalyst speeding the approach to equilibrium during garnet breakdown (Hunter & Taylor, 1982; Brearley & Scarfe, 1986; Rubie, 1986; Rubie & Brearley, 1987; Špaček *et al.*, 2013) and the present experiments demonstrate that this does, indeed play a role in garnet breakdown following Reaction 1.

As described in results, at low temperatures (1050°C), melting appears not to be required during garnet breakdown. This coincided when a switch in breakdown reaction from Reaction 1 to 2 is observed in the same experiment (E17-059). Experiments at lower temperatures of 1000°C produced a kelyphite following Reaction 2, completely absent of a melt phase, over an experimental duration of 5 days (G18-004). We interpret this to be the very first signs of equilibrium breakdown in a regime without melting. Under such conditions, breakdown kinetics are considerably slower, as would be expected in a solid-state regime.

Kinetics of reaction

The thickness of reaction rims, defined here as the region between the retrogressed garnet front and San Carlos olivine, were used as a measure of reaction progress. Reaction rim thickness was measured from BSE micrographs. Reaction kinetics were determined for the growth of Zones 1 and 2 combined, as these produce

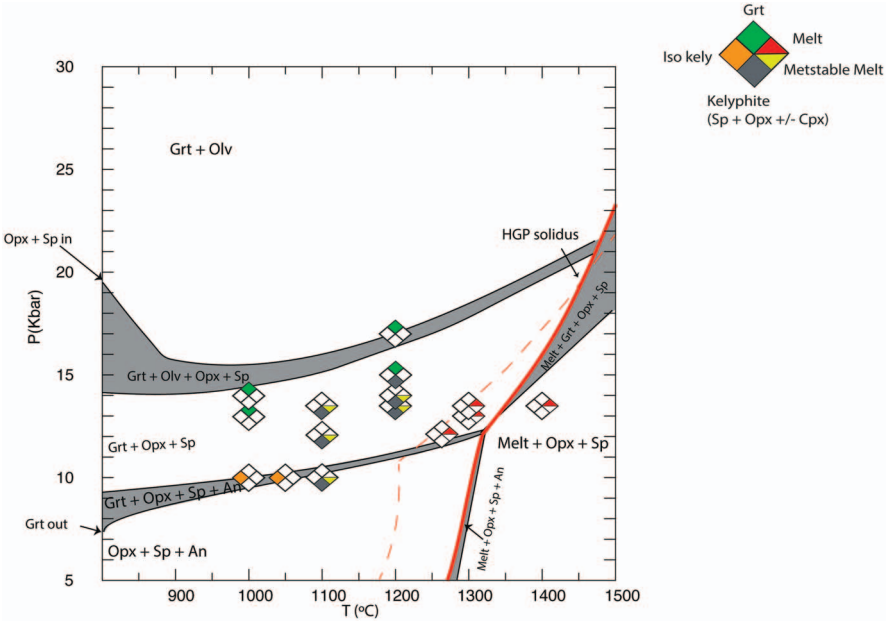

Fig. 13. Perple_X calculated pseudosection for a bulk composition of 90:10 garnet:olivine, as determined by mass balance calculations. The thick red line is the thermodynamically calculated solidus for this bulk composition, while the dashed red line shows the position of the calculated solidus for KLB-1, from solution models of Holland *et al.* (2018). Diamonds show the assemblage recovered from the longest duration experiment at a given PT condition; olivine is present in all recovered assemblages. Experiments reproduce the thermodynamically calculated stable phases in each of the phase fields, within experimental errors of pressure and temperature.

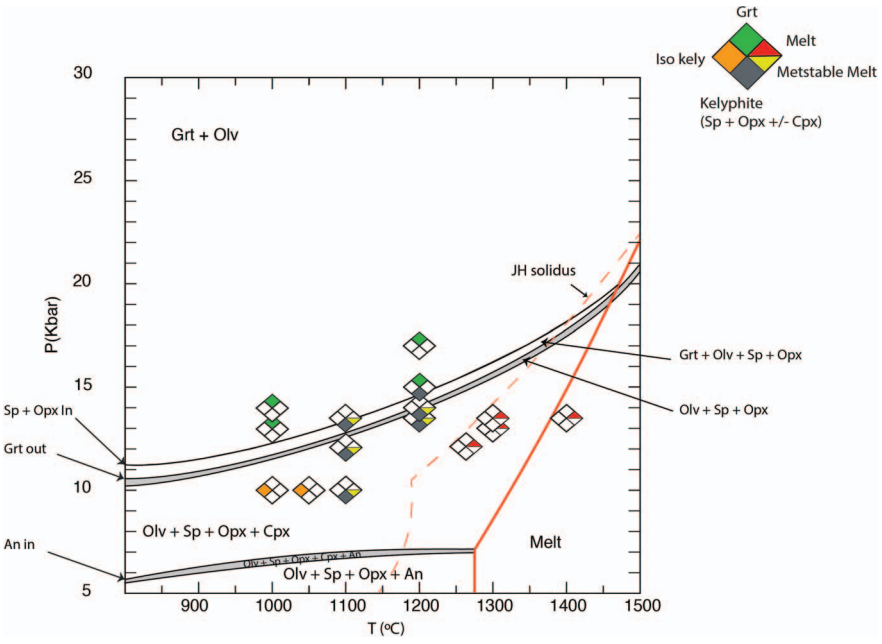

Fig. 14. Perple_X calculated pseudosection for a bulk composition of 10:90 garnet:olivine. All symbols represent the same experiments as in Fig 13, within an olivine – saturated bulk system, with a thick red line for the solidus and a dashed line for the solidus of Jennings & Holland (2015). The garnet out curve significantly increases in pressure as compared to Fig. 13, while the phase field for Olv + Sp + Opx + Cpx expands in pressure space. The solidus shifts to higher temperatures as would be expected for an assemblage with a greater bulk proportion of olivine. Experiments conducted here, fall within phase fields of the observed reaction products.

the same modal abundance of spinel, pyroxene and melt. Clearly there is a switch in both the type and kinetics of the reaction when Zones 3 and 4 are produced; however, garnet was almost entirely consumed in experiments containing Zone 4 products and so kinetic parameters for these zones were not determined.

The reaction products generally display sharp irregular boundaries with the garnet front, meaning that multiple measurements of distance, perpendicular to the original garnet–olivine interface, need to be made to provide reliable average rim thickness. Approximately 250–300 measurements of Zone1 + Zone 2 rim thicknesses were taken from multiple (2–5) images per sample, using the NIH-image J software package (Schneider *et al.*, 2012). The mean rim width, where determined (i.e. where a granular reaction rim was recovered), is reported in Table 2.

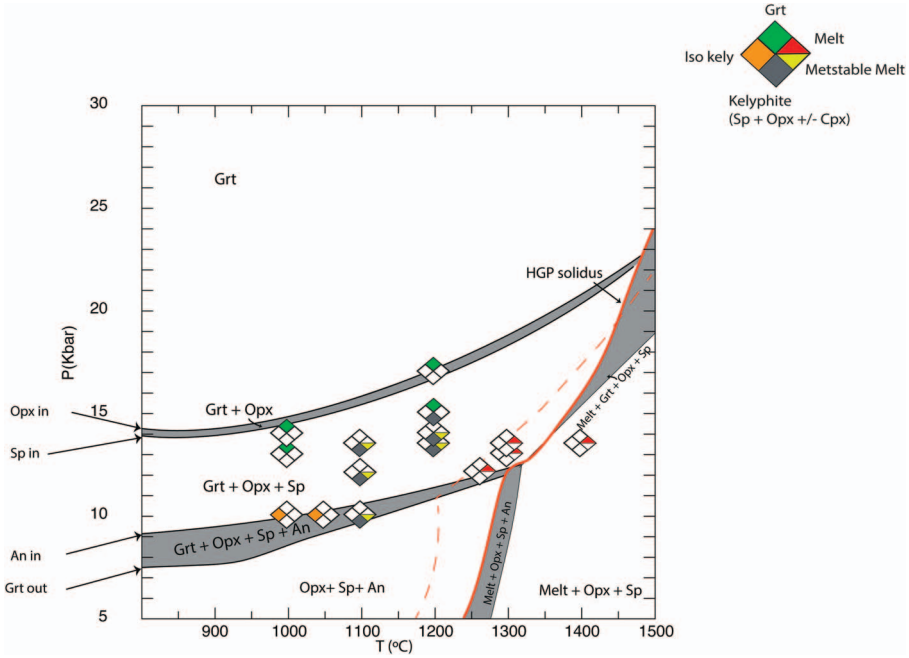

Fig. 15. Perple_X calculated pseudosection for a bulk composition of 100% garnet. The position of the solidus is almost identical to that for a bulk assemblage of 90:10 garnet:olivine. The position of an 'isochemical' assemblage of Opx + Sp + An is expanded and our experiments reproduce this assemblage to within the experimental errors of pressure and temperature for cases where no melt is produced during the experiments. Diamonds show the assemblage recovered from the longest duration experiment at a given PT condition, olivine is present in all recovered assemblages.

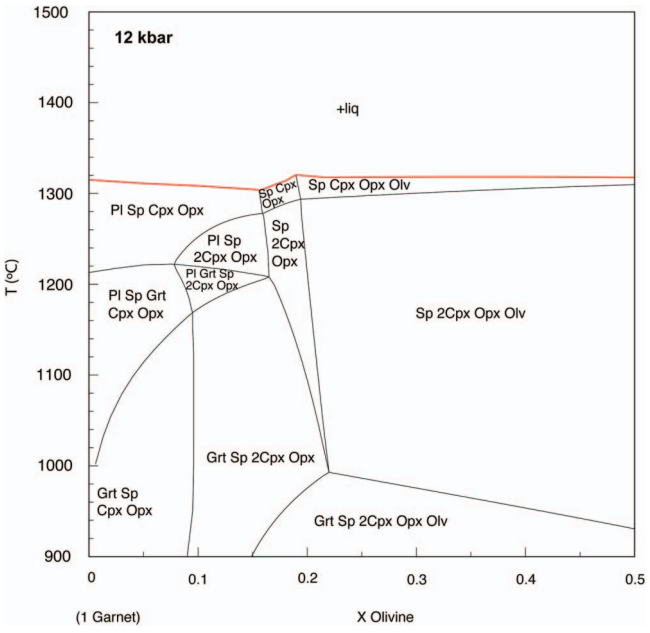

Fig. 16. THERMOCALC-calculated T-X section for bulk compositions from 100% garnet to 50:50 garnet:olivine at 12 kbar, based on the analysed compositions of Table 1. The position of the equilibrium solidus is not dramatically affected by varying ratios of garnet:olivine, suggesting an equilibrium melt is not predicted to form for the experimental starting materials presented here. 2Cpx regions are where phase separation of clinopyroxene into a low-Ca Cpx and high-Ca Cpx occurs. Single phase clinopyroxene in the T-X section have low Ca concentrations similar in composition to the clinopyroxene in the experimental charges.

Reaction rim widths were fitted to modified rate Equations 3 and 4, as described by (Pattison *et al.*, 2011):

$$[x]^2 = kt \tag{3}$$

where x is reaction rim width and t is time. The reaction rate constant, k, has an Arrhenius dependence in the form:

$$k = k_0 . \left(1 - \exp\left(\frac{A}{RT}\right)\right) . \left(\exp\left(\frac{-\Delta H}{RT}\right)\right), \tag{4}$$

where k_0 is a pre-exponential constant, H is apparent activation enthalpy, T is temperature, R is the gas constant and A is an affinity term. The affinity term is required to account for the overstep in pressure during nucleation and growth of product phases.

$$A = \Delta P . (-\Delta V), \tag{5}$$

where ΔP is the overstep in pressure from the equilibrium boundary, determined from the calculated pseudosections for compositions of garnet and olivine used in this study (see next section) and ΔV is the volume change of reaction.

A weighted least squares regression to Equation 4, in combination with a Monte Carlo calculation, for error estimation, was used to determine kinetic parameters. The regression had seven free parameters: reaction enthalpy (ΔH), k_0 and a separate variable for the apparent rim thickness at $t = 0$ for each temperature series. Errors in the parameters were calculated by Monte Carlo sampling of the experimental data (pressure, temperature, time, rim thickness and their associated uncertainties) assuming an error of 0.1 GPa in the overstep pressure (ΔP). The model is fit to resampled data 10^4 times, providing sufficient convergence of the kinetic parameters. After discarding illicit values (e.g. negative rim thicknesses) the following kinetic parameters were returned; ΔH_a =

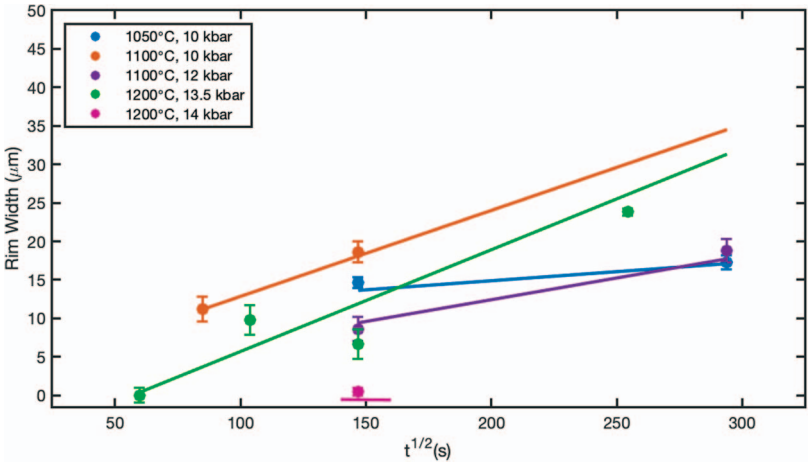

Fig. 17. Experimental reaction rim width as a function of the square root of time. Straight lines are the best fitting solution of a global regression to Equation 3.

$286 \pm 145 kJ/mol^{-1}$ and $\log k_0^{\dagger} = 11.9 \pm 5.5$ (Supplementary Fig. 1, Fig. 17).

Given the large uncertainties in the reported kinetic parameters here, it is not possible to unequivocally determine the rate limiting mechanism. However it is possible that diffusion of Mg is the rate limiting species, as it is required externally by garnet to ensure continual equilibrium breakdown (Fig. 16b). The activation enthalpies of Mg diffusion in orthopyroxene and garnet are similar to the activation enthalpy determined here, suggesting solid-state diffusion could be rate limiting to garnet breakdown ($\Delta H_{Mg}^{Opx} = 299 \pm 65 kJ/mol^{-1}$ and $\Delta H_{Mg}^{Grt} = 228 \pm 20 kJ/mol^{-1}$) (Borinski *et al.*, 2012; Dohmen *et al.*, 2016).

However several lines of evidence suggest the melt is the rate determining mechanism, aside from its observation in all high temperature experiments, the activation enthalpy is indicative of Mg diffusion during olivine dissolution in basalt; $\Delta H_{Mg}^{basalt\ (olv\ diss)} = 218 \pm 21$ (Chen & Zhang, 2008). While the melt was not identified as being in direct contact with olivine, it is likely that thin films (below the resolution of SEM-imaging) of melt exist on grain boundaries in contact with olivine and assist with Mg transport to the reaction front with garnet. Additionally, the temperature dependence of rim growth determined here ($\Delta H_a = 286 \pm 145 kJ/mol^{-1}$) is significantly smaller than rim growth of orthopyroxene ($426 \pm 34 kJ/mol^{-1}$) between quartz and olivine, in the absence of any melt (Fisler *et al.*, 1997; Milke *et al.*, 2007).

Due to the large uncertainty in the kinetic parameters presented here it is unclear which of these mechanisms, is rate limiting. Nevertheless, observations of melting and rapid reaction rates as compared to other upper mantle rim forming reactions (Fisler *et al.*, 1997; Milke *et al.*, 2007) demonstrates the importance melt has on enhancing reaction kinetics.

While we are unable to uniquely identify the rate limiting mechanism, the kinetic reaction rates can be used to determine *PTt* (pressure–temperature–time) pathways of garnet breakdown and exhumation, as will be presented in the following section.

DISCUSSION

A model for garnet breakdown

It is well documented that natural kelyphites result from Reaction 1 (Grt + Olv = Sp + Opx; (Reid & Dawson, 1972; Lock & Dawson, 1980; Medaris *et al.*, 2005; Obata, 2011), and the presence of concentric kelyphite are interpreted as evidence for multistage uplift and emplacement. The presence of melts is also well documented within kelyphite (Hunter & Taylor, 1982; Medaris *et al.*, 2005; Špaček *et al.*, 2013) but with limited interpretations as to what role, if any, melt plays during garnet breakdown. Hunter & Taylor (1982) noted the ubiquitous presence of quenched glass between the kelyphite rim and the retrogressing garnet front, as has been observed in the experiments presented here (Fig. 3), they proposed incongruent melting of garnet alone resulted in the growth of the kelyphite reaction products (spinel, orthopyroxene and clinopyroxene). The concentric kelyphite presented by Hunter & Taylor (1982) are identical to those reproduced in this study and observed elsewhere in natural samples with COR, nodular spinel and internal fine-grained intergrowths of spinel and pyroxenes (Špaček *et al.*, 2013). Similarly to other interpretations Hunter & Taylor (1982) suggested the concentric zones were formed by quenching garnet breakdown at various stages of emplacement. Here we suggest, using our experiments, that concentric kelyphite can form as a result of a series of reactions that can all occur at constant conditions of pressure and temperature.

Initially, garnet and olivine are in contact with one another, which allows Reaction 1 to take place. However, the growth of the orthopyroxene rim (COR) forms a physical barrier and isolates olivine from garnet resulting in changes in the nutrient supply, under otherwise constant conditions. Orthopyroxene formation is dependent on magnesium diffusion from the surrounding olivine towards the decomposing garnet (Obata, 2011), as described by the half-Reactions 10 and 11.

$$Mg_2SiO_4 \longrightarrow MgSiO_3 + MgO \quad (10)$$

$$MgO + Mg_3Al_2Si_2O_{12} \longrightarrow MgAl_2O_4 + 3MgSiO_3 \quad (11)$$

Instead of direct reaction, Mg must diffuse through orthopyroxene in order to reach the retreating garnet front. It is has been shown that diffusion of Mg is slower in orthopyroxene than olivine (Dohmen *et al.*, 2016) and that Mg–Fe diffusion rates of orthopyroxene are comparable to those in garnet (Dohmen *et al.*, 2016). Slower diffusion rates, coupled with increased diffusion distance may perturb Reaction 1, inducing incongruent melting of garnet.

Experimental observations suggest that once such a barrier to Reaction 1 exists, the dominant mechanism for continued garnet

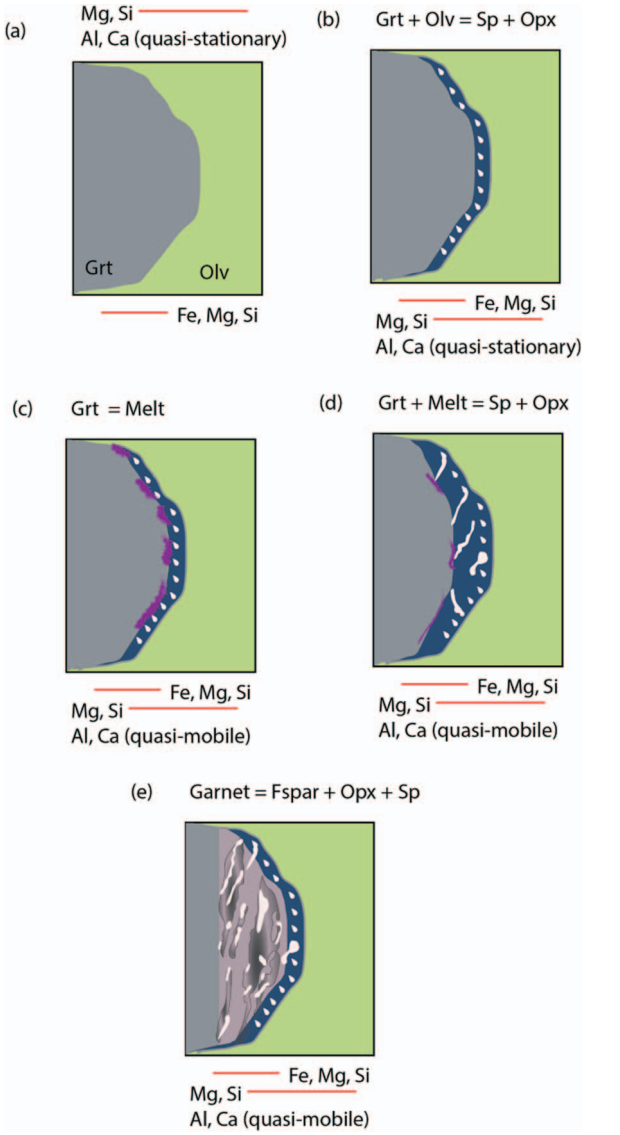

Fig. 18. Sequential corona development around garnet, following a series of reactions. Multilayer coronae develop by changes in the dominant reaction taking place, and the relative mobilities of diffusing cations. Dark blue is orthopyroxene, white spinel and pink feldspar. Corona growth begins with (b) the well understood garnet + olivine = spinel + orthopyroxene reaction. Following the growth of an orthopyroxene layer in contact with the retrogressing garnet, the reaction switches to (c) and, it is here that melting begins. The melt reacts further with garnet and olivine (d) to produce an equilibrium assemblage of spinel and orthopyroxene. (e) is an alternative reaction to the melt assisted breakdown, following Reaction 2 (garnet = spinel + orthopyroxene + anorthite +/− clinopyroxene) in the absence of olivine. This breakdown reaction can describe the textres and phases associated with Zone 4 kelyphite.

breakdown switches and garnet experiences disequilibrium melting (Equation 12) (Fig. 18c).

$$Grt = Melt \tag{12}$$

It appears the melt acts an essential diffusive agent to ensure the ongoing supply of cations to the reactive front. The requirement for diffusive assistance was also noted by Obata (2011) (Equations 13 and 14 in Obata, 2011) who suggested 'hypothetical mobile component(s)' were both produced and consumed at the reaction front. Obata (2011) also suggested local variations in kelyphite, commonly observed in nature, and implied a crucial role of fluids during kelyphitisation (Obata, 2011). We believe our identification of melting provides the first experimental verification of these hypotheses.

We observed the interaction of melt with reaction products via Equations 13a or 13b:

$$Melt = Sp + Opx \pm Cpx \tag{13a}$$

$$Melt = Olv + Fspar + Sp \tag{13b}$$

Most frequently melt reactions appear to proceed via Reaction 13a, producing spinel and orthopyroxene (occasional clinopyroxene) at the melt interface (Fig. 4 and 18d), as also described by Hunter & Taylor (1982). Where complete melt crystallisation is believed to have occurred, evidence for the former presence of melt remains in the form of faceted edges of spinel and pyroxene grains as also observed in natural kelyphite (Hunter & Taylor, 1982; Brearley & Scarfe, 1986; Špaček *et al.*, 2013).

Products corresponding to Reaction 13b (Zone 3) were observed in two experiments at 1100°C and 12 kbar (Fig. 5 & 17e). Longer duration experiments (> 6 hours) at the same conditions followed 13a, consistent with the equilibrium phase diagram. This suggests that Reaction 13a can occur as a local reequilibration process within the volume of garnet; a process that will be rapid compared to reaction with surrounding olivine because diffusive path lengths are short in the case of local reequilibration. Obata *et al.* (2014) also observed an experimental assemblage of spinel + olivine + feldspar, interpreting it as a metasomatic kelyphite requiring the introduction of external fluids. Given there was no free fluid in our experiments and they do not contain internal isochemical kelyphite an alternative mechanism must explain their presence in this study. Špaček *et al.* (2013) also observed an assemblage of spinel, feldspar and olivine, contained within kelyphite, interpreting its presence to the interaction of both *in situ* and external melts with primary reaction products of spinel and pyroxenes. However, without further detailed investigation it is challenging to evaluate the importance of Zone 3 with respect to the reactions governing garnet breakdown, and it is only rarely is observed in natural kelyphite (Špaček *et al.*, 2013).

The simple sequential breakdown reactions discussed above adequately describe the multilayer corona observed in the experiments here. We observe that at temperatures above 1000°C garnet is entirely replaced by a spinel lherzolite assemblage in a matter of hours.

The presence of quenched siliceous melt pockets in natural kelyphite coronae are also well documented (Carswell & Dawson, 1970; Reid & Dawson, 1972; Lock & Dawson, 1980; Hunter & Taylor, 1982; Mukhopadhyay, 1991; Ackerman *et al.*, 2013; Špaček *et al.*, 2013), supporting the relevance of the melt-mediated reactions documented above. However, there are important differences between the melt generated in our experiments and those observed in natural garnet peridotite (Hunter & Taylor, 1982). Glasses preserved within garnet kelyphite often have enrichments in alkalis and volatiles, exceeding those in the glasses analysed here, suggesting metasomtic melting may have contributed to garnet breakdown in mantle xenoliths (Hunter & Taylor, 1982; Špaček *et al.*, 2013). The experiments presented here however do not contain any excess alkalis as only well characterised garnet and olivine were used as starting materials (Table 1), in addition the presence of trace quantities of water (Supplementary Fig. 2) did not promote metasomatic melting, and instead we suggest that simply disequilibrium melting of garnet occurred.

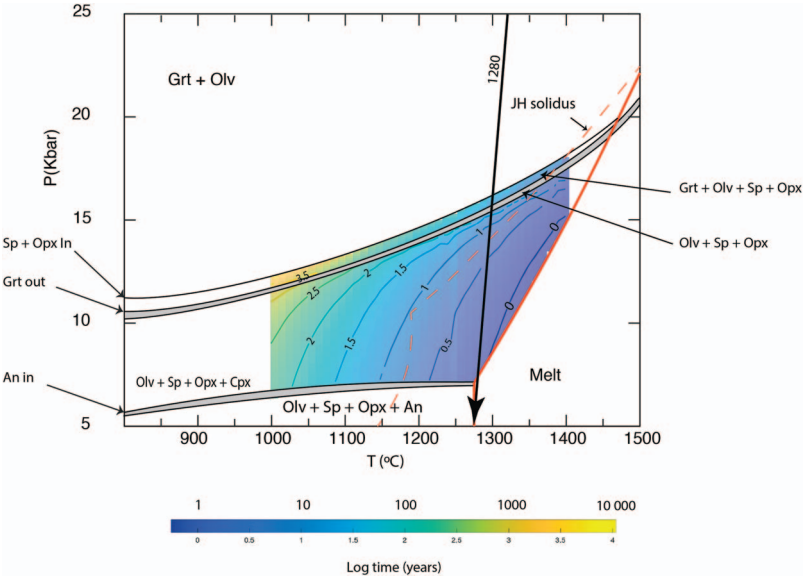

Fig. 19. Timescales for the generation of a 2.5-mm reaction rim consisting of Zones 1 and 2 while preserving an interior relic garnet. Timescales were generated using the experimentally determined reaction kinetics, across the PT conditions of garnet breakdown investigated in this study and superimposed on the 10:90 garnet:olivine thermodynamically determined pseudosection. Garnet breakdown is rapid and emplacement timescales of less than 10 000 years are required to successfully emplace kelyphite bearing mantle xenoliths to the surface and preserve a relict garnet interior. Time is in log years and a function of overstep from the equilibrium boundary of spinel to garnet lherzolite, pressure and temperature.

Garnet breakdown does not occur solely via Reactions 12 and 13; in some cases, garnet breaks down via Reaction 2. Kelyphite (Zone 4, spinel, orthopyroxene and anorthite) were observed in experiments at temperature and pressure conditions of 1000–1050°C and 10 kbar, where no melt was observed. The breakdown of garnet under these conditions is consistent with the phase boundaries determined in the garnet only pseudosection, when considered alongside experimental uncertainties in pressure and temperature (Fig. 15). Due to the fine-grained texture of Zone 4 kelyphite, chemical analysis was unable to accurately determine whether the reaction products formed through isochemical breakdown alone. The textures and thermodynamic modelling however suggest these kelyphite may be isochemical.

Short duration experiments at 1050°C possess poorly developed COR alongside frozen pockets of melt, but have no internal isochemical-like kelyphite. Conversely, longer duration experiments have both poorly developed COR and the presence of internal kelyphite but are absent of melt pockets. The incongruent melting mechanism does not appear to interfere with the development of Zone 4 kelyphite, in agreement with Obata *et al.* (2014) who also reported internal isochemical kelyphite bounded by a concentric corona.

Kelyphite formed via Reaction 2 (both isochemical and non-isochemical) have been observed in multilayer corona within garnet pyroxenite and peridotite xenoliths (Keankeo *et al.*, 2000; Dégi *et al.*, 2010; Obata *et al.*, 2013). Obata *et al.* (2013) suggested the reaction mode switches in response to a combined decrease in chemical potential gradients, increasing corona thickness and an increase in internal stresses due to the associated volume change of Reaction 1. Kelyphite formed via Reaction 2 only require local diffusion, over length scales of less than 1 μm; this seems much more efficient than limited diffusion across a COR rim, present between olivine and garnet. It appears that once Reaction 2 begins kelyphite assemblages nucleate and growth proceeds quickly, with layers of 100 μm or more formed in 2 days at 1050°C, entirely consuming the original garnet (Fig. 6).

Previous studies have generally ascribed the switch (from Reaction 1 to 2) in kelyphite formation to changes in imposed *PT* conditions during xenolith ascent through the lithospheric mantle (Keankeo *et al.*, 2000). However, our experiments conclusively demonstrate this switch may also occur in response to changes in diffusion rates at static *PT* conditions, removing the requirement for complex *PTt* pathways to explain multilayer, multiphase corona (Keankeo *et al.*, 2000; Obata *et al.*, 2013).

At temperatures below 1000°C no reactions were observed, over the experimental durations of this study. At these conditions, in the investigated periods, solid-state breakdown via Reaction 1 was too slow to proceed (even in the presence of trace H_2O). Instead, garnet breakdown occurred exclusively via Reaction 2 (Fig. 12). The lack of any outer reaction rims are indicative of the minimum temperature required for Reaction 1 (grt + olv) to proceed. As we are unaware of any mantle xenoliths that exclusively contain isochemical–kelyphite assemblages without coronae, we suggest that external fluids may act as metasomatic agents at low temperatures (below 1000°C), triggering the observed non-isochemical breakdown of garnet (Carswell & Dawson, 1970; Hunter & Taylor, 1982; Mukhopadhyay, 1991; Ackerman *et al.*, 2013; Špaček *et al.*, 2013). Alternatively mantle xenoliths with both isochemical and non-isochemical kelyphite could be the result of multistage uplift events.

Emplacement timescales for garnet bearing peridotite

We have used our experimentally determined rate of coronae growth to estimate emplacement times for a 5-mm garnet, producing a 2.5-mm reaction corona consisting of Zones 1 and 2 (Fig. 19). In order to preserve an internal garnet from an initially 5-mm diameter crystal, emplacement times from the spinel lherzolite stability field to the surface must be less than 10 000 years at a potential temperature of 1000°C (Fig. 19). This is ten times faster than ambient mantle upwelling today (Lundstrom *et al.*, 1998; Anderson *et al.*, 2014), and most likely requires a magmatic mech-

anism to emplace mantle xenoliths while preserving kelyphite textures (Obata, 1980; Ackerman *et al.*, 2013; Špaček *et al.*, 2013).

Garnet bearing xenoliths have been transported to the surface almost exclusively in unusual magmas such as kimberlites, which do not occur today, requiring special geodynamic settings (Reid & Dawson, 1972; Canil & Fedortchouk, 1999; Sparks, 2013). The potential temperature of kimberlitic melts carrying mantle xenoliths is approximated at 1310–1380°C (Kavanagh & Sparks, 2009), at these high temperatures emplacement of garnet with kelyphitic textures would need to occur in substantially less than 1 year, based on the experimental results presented here (Fig. 18). Estimates of kimberlite ascent rates also range from a few hours, 1–10 experimentally determined by dissolution of garnet in kimberlite magma (Canil & Fedortchouk, 1999), to less than 1 hour when assessing hydrogen diffusion in olivine from mantle xenoliths (Peslier *et al.*, 2008). Timescales of less than one year in the order of a few hours to a day are in good agreement with those determined by the reaction kinetics of garnet breakdown presented here. Rapid emplacement times, of ~1 year, are also required for alkali basalts erupting at surface temperatures of 1210–1280°C, consistent with previous studies (Green *et al.*, 1967; Brearley & Scarfe, 1986). Reconstructed *PT* estimates, of natural kelyphite, also suggest rapid emplacement of mantle xenoliths with last equilibrated conditions from within the garnet lherzolite stability field (1120°C and 14.9 kbar; Dégi *et al.*, 2010).

The predictions, made here, on emplacement time are controlled by the presence of melt and, while there appears to be compelling evidence for breakdown of garnet by reaction with *external* melts (Carswell & Dawson, 1970; Reid & Dawson, 1972; Lock & Dawson, 1980; Hunter & Taylor, 1982; Mukhopadhyay, 1991; Ackerman *et al.*, 2013; Špaček *et al.*, 2013), we show that garnet breakdown may also occur in the absence of such melts (Zone 4 textures). The presence of external reactive melts might further enhance reaction rates meaning that the present experiments can only place upper bounds on transit and emplacement times.

These rapid emplacement times imply an uninterrupted passage through the mantle is required from the entrainment of mantle xenoliths (depths of ~60 km) to the surface. Complex multilayered coronae might be produced by a two-stage process of emplacement of xenolith-bearing mantle melts into mid-lower crust. The low ambient temperatures in the crust would result in a switch of decomposition mechanism from a melt-mitigated process to one of isochemical breakdown. This is consistent with natural garnet xenoliths with Zone 4 textures (both isochemical and non-isochemical), which yield low reconstructed *PT* conditions at 650–980°C and 9–15 kbar (Mukhopadhyay, 1991; Ionov *et al.*, 1993; Godard & Martin, 2000). A process of melt stagnation, freezing and remelting may be the only mechanism by which to generate complex multilayered coronae as the emplacement temperatures from kimberlites and alkali basalts are too high to otherwise induce multilayered coronae growth.

CONCLUSIONS

Garnet bearing mantle xenoliths host kelyphitic textures, resulting from incomplete garnet re-equilibration in the spinel lherzolite stability field. Kelyphitic coronae provide insight into the behaviour of the mantle during uplift and exhumation.

We performed high pressure, high temperature experiments on natural garnet to recreate kelyphitic coronae, in order to determine the reaction kinetics of garnet breakdown in the mantle.

Our experiments reproduce an array of kelyphitic textures, similar to those found in natural mantle xenoliths (Reid & Dawson, 1972; Lock & Dawson, 1980; Dégi *et al.*, 2010; Obata & Ozawa, 2011; Špaček *et al.*, 2013). Importantly our results demonstrate garnet breakdown is not a simple single reaction process as previously assumed, and it is best described as a series of cascading reactions beginning with the well understood olivine + garnet reaction. Once initiated garnet appears to breakdown rapidly via incongruent melting following our newly presented Reactions 12 and 13, at least at high temperatures above 1000°C.

The breakdown of garnet is assisted by the presence of a melt phase. Silicate melt is present in nearly all our experiments at temperatures above 1000°C. This melt is an essential catalyst to garnet breakdown which does not alter the final equilibrium assemblage and is likely completely consumed upon attainment of equilibrium.

The occurrence of several reactions, some of which are assisted by melt, makes determination of reaction kinetics in experiments challenging. Despite difficulties, we present reaction kinetics describing the dissolution of garnet and subsequent growth of opx + sp ± cpx coronae; a partial description of garnet breakdown. Kinetic results provide an indication that magnesium diffusion in melt may potentially be the rate limiting mechanism during garnet breakdown beginning with Reaction 1. The empirically derived activation enthalpy of $\Delta H_a = 286 \pm 145$ kJ/mol^{-1} for combined growth of Zone 1 and 2 textures is similar to that of magnesium diffusion in melt and orthopyroxene (Zhang *et al.*, 2010; Borinski *et al.*, 2012; Dohmen *et al.*, 2016) but rates of reaction in the presence of melt are sufficiently fast to make diffusion in the liquid state the most likely mechanism.

Incongruent melting of garnet has also been reported elsewhere as a possible mechanism for kelyphite formation (Hunter & Taylor, 1982; Brearley & Scarfe, 1986; Špaček *et al.*, 2013). Evidence for the involvement of melt/fluids in the retrogression of mantle samples suggests natural kelyphitisation is likely to follow similar kinetics and reactions to those seen in the present experiments. The cascade of reactions, presented here, produces distinctive multizoned, multiphase textures, which are similar to those found in natural mantle xenoliths. Multilayered corona common in nature can be produced at constant conditions of pressure and temperature, removing the need to interpret complex *PTt* pathways of exhumation (Mukhopadhyay, 1991; Atzori *et al.*, 1999; Godard & Martin, 2000; Guo *et al.*, 2002; Dégi *et al.*, 2010; Obata *et al.*, 2013; Špaček *et al.*, 2013). However, some of the primary reaction textures from initial garnet breakdown in natural xenoliths are expected to be overprinted by continued metamorphism and/or retrogression at subsequent (lower pressure) conditions. These later processes, which likely overprint primary textures, may make the identification of melts from garnet breakdown almost impossible. Experiments provide a frozen snapshot of the partially complete kelyphitisation process and therein preserve features which are lost to continued breakdown and re-equilibration in the spinel lherzolite field.

To preserve relict garnets in the core of kelyphite requires emplacement from depths of the spinel lherzolite stability field (30–50 km) to the surface on timescales of 1–10 000 years for mantle potential temperatures of 1000–1280°C.

At temperatures below 1000°C, where there is no melting of garnet, its breakdown produces kelyphite textures with an average composition which is close to the parent garnet. We have not constrained the kinetics of this solid-state breakdown but note that it must be substantially slower than the melt-catalysed high-T reaction since we only reproduced this texture in a single

long duration (168 hour) experiment. The low temperature experiments suggest that the solid state growth of Zone 4 kelyphite is initially kinetically inhibited by a nucleation barrier but once new phases have nucleated rather rapid eutectoid-type breakdown can occur.

DATA AVAILABILITY

The data underlying this article are available in the article and in its online supplementary material.

SUPPLEMENTARY DATA

Supplementary data are available at *Journal of Petrology* online.

ACKNOWLEDGEMENTS

We thank James Davy for assistance with SEM imaging at UCL and Elisabetta Mariani for scientific discussions and assistance with EBSD at University of Liverpool. This work was part of ISE's NERC-funded PhD.

FUNDING

This work was supported by the Natural Environment Research Council [NE/Mooo46x/1 to J.B. and D.D.].

References

Ackerman, L., Špaček, P., Magna, T., Ulrych, J., Svojtka, M., Hegner, E. & Balogh, K. (2013). Alkaline and carbonate-rich melt metasomatism and melting of subcontinental lithospheric mantle: evidence from mantle xenoliths, ne Bavaria, bohemian massif. *Journal of Petrology* **54**, 2597–2633. https://doi.org/10.1093/petrology/egt059.

Ai, Y. (1994). A revision of the garnet-clinopyroxene Fe2+-Mg exchange geothermometer. *Contributions to Mineralogy and Petrology* **115**, 467–473. https://doi.org/10.1007/BF00320979.

Anderson, D. L., Natland, J. H. & Ernst, W. G. (2014). Mantle updrafts and mechanisms of oceanic volcanism. *Proceedings of the National Academy of Sciences of the United States of America* **111**, E4298–E4304. https://doi.org/10.1073/pnas.1410229111.

Atzori, P., Mazzoleni, P., Punturo, R. & Scribano, V. (1999). Garnet-spinel-pyroxenite xenoliths from Hyblean Plateau (South-Eastern Sicily, Italy). *Mineralogy and Petrology* **66**, 215–226. https://doi.org/10.1007/bf01164494.

Basu, A. R. & MacGregor, I. D. (1975). Chromite spinels from ultramafic xenoliths. *Geochimica et Cosmochimica Acta* **39**, 937–945. https://doi.org/10.1016/0016-7037(75)90039-3.

Bjerg, E. A., Ntaflos, T., Thöni, M., Aliani, P. & Labudia, C. H. (2009). Heterogeneous lithospheric mantle beneath Northern Patagonia: evidence from Prahuaniyeu garnet- and spinel-peridotites. *Journal of Petrology* **50**, 1267–1298. https://doi.org/10.1093/petrology/egp021.

Borinski, S. A., Hoppe, U., Chakraborty, S., Ganguly, J. & Bhowmik, S. K. (2012). Multicomponent diffusion in garnets I: general theoretical considerations and experimental data for Fe-Mg systems. *Contributions to Mineralogy and Petrology* **164**, 571–586. https://doi.org/10.1007/s00410-012-0758-0.

Brearley, M. & Scarfe, C. M. (1986). Dissolution rates of upper mantle minerals in an alkali basalt melt at high pressure: an experimental study and implications for ultramafic xenolith survival. *Journal of Petrology* **27**, 1157–1182. https://doi.org/10.1093/petrology/27.5.1157.

Canil, D. & Fedortchouk, Y. (1999). Garnet dissolution and the emplacement of kimberlites. *Earth and Planetary Science Letters* **167**, 227–237. https://doi.org/10.1016/S0012-821X(99)00019-9.

Carswell, D. A. & Dawson, J. B. (1970). Garnet peridotite xenoliths in south African kimberlite pipes and their petrogenesis. *Contributions to Mineralogy and Petrology* **25**, 163–184. https://doi.org/10.1007/BF00371129.

Chakraborty, S. & Ganguly, J. (1992). Cation diffusion in aluminosilicate garnets: experimental determination in spessartine-almandine diffusion couples, evaluation of effective binary diffusion coefficients, and applications. *Contributions to Mineralogy and Petrology* **111**, 74–86. https://doi.org/10.1007/BF00296579.

Chen, Y. & Zhang, Y. (2008). Olivine dissolution in basaltic melt. *Geochimica et Cosmochimica Acta* **72**, 4756–4777. https://doi.org/10.1016/j.gca.2008.07.014.

Clarke, G. L. & Powell, R. (1991). Decompressional coronas and symplectites in granulites of the Musgrave complex, Central Australia. *Journal of Metamorphic Geology* **9**, 441–450. https://doi.org/10.1111/j.1525-1314.1991.tb00538.x.

Connolly, J. A. D. (2009). The geodynamic equation of state: what and how. *Geochemistry, Geophysics, Geosystems* **10**. https://doi.org/10.1029/2009GC002540.

Dégi, J., Abart, R., Török, K., Bali, E., Wirth, R. & Rhede, D. (2010). Symplectite formation during decompression induced garnet breakdown in lower crustal mafic granulite xenoliths: mechanisms and rates. *Contributions to Mineralogy and Petrology* **159**, 293–314. https://doi.org/10.1007/s00410-009-0428-z.

Dohmen, R., ter Heege, J. H., Becker, H. W. & Chakrabortrty, S. (2016). Fe-mg interdiffusion in orthopyroxene. *American Mineralogist* **101**, 2210–2221. https://doi.org/10.2138/am-2016-5815.

Fisler, D. K., Mackwell, S. J. & Petsch, S. (1997). Grain boundary diffusion in enstatite. *Physics and Chemistry of Minerals* **24**, 264–273. https://doi.org/10.1007/s002690050038.

Godard, G. & Martin, S. (2000). Petrogenesis of kelyphites in garnet peridotites: a case study from the Ulten zone, Italian Alps. *Journal of Geodynamics* **30**, 117–145. https://doi.org/10.1016/S0264-3707(99)00030-7.

Green, T. H., Green, D. H. & Ringwood, A. E. (1967). The origin of high-alumina basalts and their relationships to quartz tholeiites and alkali basalts. *Earth and Planetary Science Letters* **2**, 41–51. https://doi.org/10.1016/0012-821X(67)90171-9.

Grégoire, M., Tinguely, C., Bell, D. R. & le Roex, A. P. (2005). Spinel lherzolite xenoliths from the premier kimberlite (Kaapvaal craton, South Africa): nature and evolution of the shallow upper mantle beneath the Bushveld complex. *Lithos* **84**, 185–205. https://doi.org/10.1016/j.lithos.2005.02.004.

Guo, J. H., O'Brien, P. J. & Zhai, M. (2002). High-pressure granulites in the Sanggan area, North China craton: metamorphic evolution, P-T paths and geotectonic significance. *Journal of Metamorphic Geology* **20**, 741–756. https://doi.org/10.1046/j.1525-1314.2002.00401.x.

Holland, T. J. B. (1980). The reaction albite= jadeite+ quartz determined experimentally in the range 600-1200 degrees C. *American Mineralogist* **65**, 129–134 http://ammin.geoscienceworld.org/content/65/1-2/129.short.

Holland, T. J. B. & Powell, R. (2011). An improved and extended internally consistent thermodynamic dataset for phases of petrological interest, involving a new equation of state for solids. *Journal of Metamorphic Geology* **29**, 333–383. https://doi.org/10.1111/j.1525-1314.2010.00923.x.

Holland, T. J. B., Green, E. C. R. & Powell, R. (2018). Melting of peridotites through to granites: a simple thermodynamic model in the system KNCFMASHTOCr. *Journal of Petrology* **59**, 881–900. https://doi.org/10.1093/petrology/egy048.

Hunter, R. H. & Taylor, L. A. (1982). Instability of garnet from the mantle: glass as evidence of metasomatic melting. *Geology* **10**, 617–620. 10.1130/0091-7613(1982)10<617:IOGFTM>2.0.CO;2.

Ionov, D. A., Ashchepkov, I. V., Stosch, H. G., Witt-eickschen, G. & Seck, H. A. (1993). Garnet peridotite xenoliths from the vitim volcanic field, baikal region: the nature of the garnet-spinel peridotite transition zone in the continental mantle. *Journal of Petrology* **34**, 1141–1175. https://doi.org/10.1093/petrology/34.6.1141.

Irifune, T. (1987). An experimental investigation of the pyroxene-garnet transformation in a pyrolite composition and its bearing on the constitution of the mantle. *Physics of the Earth and Planetary Interiors* **45**,324–336.https://doi.org/10.1016/0031-9201(87)90040-9.

Jennings, E. S. & Holland, T. J. B. (2015). A simple thermodynamic model for melting of peridotite in the system NCFMASOCr. *Journal of Petrology* **56**, 869–892. https://doi.org/10.1093/petrology/egv020.

Johannes, W. (1980). Metastable melting in the granite system Qz-Or-Ab-An-H2O. *Contributions to Mineralogy and Petrology* **72**, 73–80. https://doi.org/10.1007/BF00375569.

Karato, S., Wang, Z., Liu, B. & Fujino, K. (1995). Plastic deformation of garnets: systematics and implications for the rheology of the mantle transition zone. *Earth and Planetary Science Letters* **130**, 13–30. https://doi.org/10.1016/0012-821X(94)00255-W.

Kavanagh, J. L. & Sparks, R. S. J. (2009). Temperature changes in ascending kimberlite magma. *Earth and Planetary Science Letters* **286**, 404–413. https://doi.org/10.1016/j.epsl.2009.07.011.

Kawai, N. & Endo, S. (1970). The generation of ultrahigh hydrostatic pressures by a split sphere apparatus. *Review of Scientific Instruments* **41**, 1178–1181. https://doi.org/10.1063/1.1684753.

Keankeo, W., Taylor, W. R. & Fitzgerald, J. D. (2000). Clinoferrosilite-bearing kelyphite: a breakdown product of xenolithic garnet, delegate breccia pipes, New South Wales, Australia. *Mineralogical Magazine* **64**, 469–479. https://doi.org/10.1180/002646100549364.

Kushiro, I. & Yoder, H. S. (1966). Anorthite–forsterite and anorthite–enstatite reactions and their bearing on the basalt–eclogite transformation. *Journal of Petrology* **7**, 337–362. https://doi.org/10.1093/petrology/7.3.337.

Lock, N. P. & Dawson, J. B. (1980). Garnet-olivine reaction in the upper mantle: evidence from peridotite xenoliths in the Letseng-la-Terae kimberlites, Lesotho. *Earth and Environmental Science Transactions of the Royal Society of Edinburgh* **71**, 47–53. https://doi.org/10.1017/S0263593300013481.

Lundstrom, C. C., Gill, J., Williams, Q. & Hanan, B. B. (1998). Investigating solid mantle upwelling beneath mid-ocean ridges using U-series disequilibria. II. A local study at 33°S Mid-Atlantic Ridge. *Earth and Planetary Science Letters* **157**, 167–181. https://doi.org/10.1016/S0012-821X(98)00039-9.

Macgregor, I. D. (1970). The effect of CaO, Cr2O3, Fe2O3 and Al2O3 on the stability of spinel and garnet peridotites. *Physics of the Earth and Planetary Interiors* **3**, 372–377. https://doi.org/10.1016/0031-9201(70)90077-4.

Medaris, G., Wang, H., Jelínek, E., Mihaljevič, M. & Jakeš, P. (2005). Characteristics and origins of diverse Variscan peridotites in the Gföhl Nappe, Bohemian Massif, Czech Republic. *Lithos* **82**, 1–23. https://doi.org/10.1016/j.lithos.2004.12.004.

Milke, R., Dohmen, R., Becker, H. W. & Wirth, R. (2007). Growth kinetics of enstatite reaction rims studied on nano-scale, part I: methodology, microscopic observations and the role of water. *Contributions to Mineralogy and Petrology* **154**, 519–533. https://doi.org/10.1007/s00410-007-0207-7.

Mukhopadhyay, B. (1991). Garnet breakdown in some deep seated garnetiferous xenoliths from the Central Sierra Nevada: petrologic and tectonic implications. *Lithos* **27**, 59–78. https://doi.org/10.1016/0024-4937(91)90020-L.

Nagayoshi, M., Kubo, T. & Kato, T. (2016). Experimental investigation of the kinetics of the spinel-to-garnet transformation in peridotite: a preliminary study. *American Mineralogist* **101**, 2020–2028. https://doi.org/10.2138/am-2016-5586.

Obata, M. (1980). The Ronda Peridotite: garnet-, spinel-, and plagioclase-lherzolite facies and the P-T trajectories of a high-temprature mantle intrusion. *Journal of Petrology* **21**, 533–572. https://doi.org/10.1093/petrology/21.3.533.

Obata, M., 2011. Kelyphite and symplectite: textural and mineralogical diversities and universality, and a new dynamic view of their structural formation. In: Sharkov, E. V. (ed.) *New Frontiers in Tectonic Research - General Problems, Sedimentary Basins and Island Arcs*. London: InTechOpen, p. 13. https://doi.org/10.5772/20265.

Obata, M. (2016). Kelyphite and symplectite: toward a new development of the study of metamorphic reactions. *Japanese Magazine of Mineralogical and Petrological Sciences* **45**, 1–12. https://doi.org/10.2465/GKK.160108.

Obata, M. & Ozawa, K. (2011). Topotaxic relationships between spinel and pyroxene in kelyphite after garnet in mantle-derived peridotites and their implications to reaction mechanism and kinetics. *Mineralogy and Petrology* **101**, 217–224. https://doi.org/10.1007/s00710-011-0145-y.

Obata, M., Ozawa, K., Naemura, K. & Miyake, A. (2013). Isochemical breakdown of garnet in orogenic garnet peridotite and its implication to reaction kinetics. *Mineralogy and Petrology* **107**, 881–895. https://doi.org/10.1007/s00710-012-0260-4.

Obata, M., Ohi, S. & Miyake, A. (2014). Experimental synthesis of isochemical kelyphite - a preliminary report. *Journal of Mineralogical and Petrological Sciences* **109**, 91–96. https://doi.org/10.2465/jmps.131022a.

Pattison, D. R. M., de Capitani, C. & Gaidies, F. (2011). Petrological consequences of variations in metamorphic reaction affinity. *Journal of Metamorphic Geology* **29**, 953–977. https://doi.org/10.1111/j.1525-1314.2011.00950.x.

Perrillat, J. P., Daniel, I., Lardeaux, J. M. & Cardon, H. (2003). Kinetics of the coesite-quartz transition: application to the exhumation of ultrahigh-pressure rocks. *Journal of Petrology* **44**(4), 773–788. https://doi.org/10.1093/petrology/44.4.773.

Peslier, A. H., Woodland, A. B. & Wolff, J. A. (2008). Fast kimberlite ascent rates estimated from hydrogen diffusion profiles in xenolithic mantle olivines from southern Africa. *Geochimica et Cosmochimica Acta* **72**, 2711–2722. https://doi.org/10.1016/j.gca.2008.03.019.

Powell, R., Holland, T. & Worley, B. (1998). Calculating phase diagrams involving solid solutions via non-linear equations, with examples using THERMOCALC. *Journal of Metamorphic Geology* **16**, 577–588. https://doi.org/10.1111/j.1525-1314.1998.00157.x.

Reid, A. M. & Dawson, J. B. (1972). Olivine-garnet reaction in peridotites from Tanzania. *Lithos* **5**, 115–124. https://doi.org/10.1016/0024-4937(72)90063-1.

Richardson, S. H., Erlank, A. J. & Hart, S. R. (1985). Kimberlite-borne garnet peridotite xenoliths from old enriched subcontinental lithosphere. *Earth and Planetary Science Letters* **75**, 116–128. https://doi.org/10.1016/0012-821X(85)90094-9.

Rubie, D. C. (1986). The catalysis of mineral reactions by water and restrictions on the presence of aqueous fluid during metamorphism. *Mineralogical Magazine* **50**, 399–415. https://doi.org/10.1180/minmag.1986.050.357.05.

Rubie, D. C. & Brearley, A. J. (1987). Metastable melting during the breakdown of muscovite + quartz at 1 kbar. *Bulletin de Minéralogie* **110**, 533–549. https://doi.org/10.3406/bulmi.1987.7995.

Schneider, C. A., Rasband, W. S. & Eliceiri, K. W. (2012). NIH image to ImageJ: 25 years of image analysis. *Nature Methods* **9**, 671–675. https://doi.org/10.1038/nmeth.2089.

Špaček, P., Ackerman, L., Habler, G., Abart, R. & Ulrych, J. (2013). Garnet breakdown, symplectite formation and melting in basanite-hosted peridotite xenoliths from zinst (Bavaria, bohemian massif). *Journal of Petrology* **54**, 1691–1723. https://doi.org/10.1093/petrology/egt028.

Sparks, R. S. J. (2013). Kimberlite volcanism. *Annual Review of Earth and Planetary Sciences* **41**, 497–528. https://doi.org/10.1146/annurev-earth-042711-105252.

Su, B., Zhang, H., Tang, Y., Chisonga, B., Qin, K., Ying, J. & Sakyi, P. A. (2011). Geochemical syntheses among the cratonic, off-cratonic and orogenic garnet peridotites and their tectonic implications. *International Journal of Earth Sciences* **100**, 695–715. https://doi.org/10.1007/s00531-010-0527-0.

Tomlinson, E. L. & Holland, T. J. B. (2021). A thermodynamic model for the subsolidus evolution and melting of Peridotite. *Journal of Petrology* **62**(1). https://doi.org/10.1093/petrology/egab012.

Walker, D., Carpenter, M. A. & Hitch, C. M. (1990). Some simplifications to multianvil devices for high pressure experiments. *American Mineralogist* **75**, 1020–1028.

Zhang, Y., Ni, H. & Chen, Y. (2010). Diffusion data in silicate melts. *Reviews in Mineralogy and Geochemistry* **72**, 311–408. https://doi.org/10.2138/rmg.2010.72.8.